



MXene-Based Fibers, Yarns, and Fabrics for Wearable Energy Storage Devices

AUTHOR(S)

A Levitt, Jizhen Zhang, G Dion, Y Gogotsi, Joselito Razal

PUBLICATION DATE

01-11-2020

HANDLE

[10536/DRO/DU:30138030](https://hdl.handle.net/10536/DRO/DU:30138030)

Downloaded from Deakin University's Figshare repository

Deakin University CRICOS Provider Code: 00113B

MXene-Based Fibers, Yarns, and Fabrics for Wearable Energy Storage Devices

Ariana Levitt, Jizhen Zhang, Genevieve Dion,* Yury Gogotsi,* and Joselito M. Razal*

Textile devices have benefited from the discovery of new conductive materials and innovations in textile device design. These devices include textile-based supercapacitors (TSCs), encompassing fiber, yarn, and fabric supercapacitors, which have demonstrated practical value in powering wearable devices. Recent review articles have highlighted the limited energy density of TSCs as an important challenge, demanding new electrode materials with higher electronic conductivity and theoretical capacitance than present materials. $Ti_3C_2T_x$, a member of the MXene family, is known for its metallic conductivity and high volumetric capacitance in acidic electrolytes due to its pseudocapacitive behavior. Driven by these excellent properties, recent literature has reported promising integration methods of $Ti_3C_2T_x$ into TSCs with significantly improved areal and volumetric capacitance compared with non-MXene-based TSCs. Furthermore, knitted MXene-based TSCs demonstrated practical application of wearable energy storage devices in textiles. Herein, the techniques used to produce MXene-based fibers, yarns, and fabrics and the progress in architecture design and performance metrics are highlighted. Challenges regarding the introduction of this new material into fiber/yarn/fabric architectures are discussed, which will inform the development of textile-based devices beyond energy storage applications. Opportunities surrounding the development of MXene-based fibers with tunable mechanical, electrical, and electrochemical properties are proposed, which will be the direction of future research efforts.

linen, silk, etc.). In the 1800s, regenerated fibers were developed as alternatives to natural fibers with the intention of reducing costs and improving properties such as luster and drape. The development of synthetic fibers began with the discovery of nylon^[1] by Wallace Carothers at DuPont in the 1930s and shortly after, a wide range of fibers were synthesized, including polyester, Kevlar, polyacrylonitrile (PAN), and carbon fiber.^[2,3] These fibers were designed to have specific properties, such as high elasticity, mechanical strength, and thermal stability, to meet the demands of emerging textile-based applications. In the 21st century, with the rapid development of science and technology, portable and wearable devices put forward new requirements for fibers, including the ability to conduct electricity, store energy, and sense body movements.^[4–6] This resulted in a new category of fibers referred to as “functional fibers,”^[7] which are developed by incorporating highly conductive, energy storing, and mechanically strong materials, such as MXenes, an emerging family of 2D carbides, nitrides, and/or carbonitrides, into fibers (Figure 1).

1. Introduction

Fibers, yarns, and textiles have a rich history dating back thousands of years to the earliest uses of natural fibers (cotton,

By integrating functional fibers into textiles, a variety of devices have been realized, including textile-based strain sensors and pressure sensors, antennas, and heaters. These devices require high performance power systems with small size, high flexibility, and adaptability to allow for frequent deformations during use, leading to the development of textile-based supercapacitors (TSCs), including fiber-, yarn-, and fabric-based devices.


TSCs offer three main advantages for powering wearable devices over their rigid and bulky counterparts. First, TSCs demonstrate a high degree of mechanical flexibility, which helps to withstand long-term and repetitive deformations. Second, TSCs bring design versatility as they can be cut and packaged into small and diverse shapes. Third, the 1D nature of fiber-based electrodes enables integration into textiles, which is preferable for the fabrication of multifunctional wearable systems. However, the main challenge of TSCs is how to improve their energy storage capabilities. To realize their potential, TSCs require fiber-based electrode materials that demonstrate high electrical conductivity, capacitance, and energy density.

A growing number of materials have been used for TSC electrodes, including carbon-based materials (activated carbon,^[8] carbon nanotubes,^[9] and graphene^[6,10,11]), pseudocapacitive

A. Levitt, Prof. Y. Gogotsi
A. J. Drexel Nanomaterials Institute and Department
of Materials Science and Engineering
Drexel University
Philadelphia, PA 19104, USA
E-mail: gogotsi@drexel.edu

A. Levitt, Prof. G. Dion
Center for Functional Fabrics
Drexel University
Philadelphia, PA 19104, USA
E-mail: gd63@drexel.edu

J. Zhang, Prof. J. M. Razal
Institute for Frontier Materials
Deakin University
Geelong, VIC 3216, Australia
E-mail: joselito.razal@deakin.edu.au

 The ORCID identification number(s) for the author(s) of this article can be found under <https://doi.org/10.1002/adfm.202000739>.

DOI: 10.1002/adfm.202000739

nanoparticles (MnO_2 ,^[12,13] RuO_2 ,^[14–16] etc.), and intrinsically conducting polymers (polyaniline^[17] and poly(3,4-ethylenedioxythiophene):polystyrene sulfonate (PEDOT:PSS)^[18]). Carbon-based materials, the most commonly used electrodes for TSCs, are known for their high specific surface area, thermal and chemical stability, and low cost. However, these materials suffer from high resistance and have limited energy density and capacitance. In comparison, transition metal oxides offer higher specific capacitance due to their pseudocapacitive behavior achieved by the redox reactions of transition metal oxides or intercalation of ions.^[19] However, the low electrical conductivity and poor mechanical properties of these materials restrict their rate performance and limit their practical applications. Intrinsically conducting polymers are those with the most promising pseudocapacitive properties offering high capacitance but have a limited cycle life due to degradation over time. Therefore, TSCs require new electrode materials that have higher electronic conductivity and theoretical capacitance and good cycling stability compared to present materials.

A promising family of materials for the development of electrodes, current collectors, and interconnects for textile-based devices are MXenes, owing to their exciting combination of electrical, electrochemical, and mechanical properties.^[20] MXenes have the general formula $\text{M}_{n+1}\text{X}_n\text{T}_x$, where M is an early transition metal ($n = 1–4$), X represents carbon and/or nitrogen, and T_x represents the surface terminations ($-\text{O}$, $-\text{OH}$, $-\text{F}$, $-\text{Cl}$).^[21,22] Since their discovery in 2011,^[23] about 30 different stoichiometric MXenes have been synthesized and the structures and properties of dozens more have been theoretically predicted.^[24] Within the past eight years, MXenes have been used in a wide variety of applications, including, but not limited to, energy storage,^[25] water purification,^[26] electromagnetic interference (EMI) shielding,^[27] and antennas.^[28]

Of the MXenes that have been synthesized to date, $\text{Ti}_3\text{C}_2\text{T}_x$ (also referred to as MXene throughout this report) remains the most well studied. The present optimal synthesis conditions of MXene result in very high conductivity (up to $15\,000\text{ S cm}^{-1}$ as a thin film),^[29] and volumetric capacitance (up to 1500 F cm^{-3}).^[25] Besides the high electrical conductivity and energy storage performance, MXene has a hydrophilic surface, leading to good solution processability without additional binders or surfactants, which has been demonstrated by the ability to 3D print,^[30] spray-coat,^[31] spin-cast,^[32] and stamp neat MXene dispersions.^[33] Additionally, there has been a growing understanding of its rheological behavior^[34] and dispersibility in organic solvents,^[35,36] opening possibilities for processing MXenes into new architectures and geometries. The combination of these properties, along with its processability, makes MXene an attractive material for the development of functional fibers for smart textile applications.

Prompted by these properties, several studies have been dedicated to developing MXene-based fibers since their first demonstration in 2017,^[37] spanning applications from wearable energy storage^[37,38] to heated textiles,^[39] pressure sensors,^[40] and strain sensors.^[41] For energy storage applications, TSCs made from MXene-based fibers, yarns, and fabrics have demonstrated record capacitances compared to devices made from other materials, including graphene, carbon nanotubes (CNTs), and conducting polymers.^[42–44] These fibers and



Ariana Levitt is a PhD candidate and NSF-GRFP fellow pursuing a degree in Materials Science and Engineering at Drexel University, under the mentorship of Prof. Yury Gogotsi and Prof. Genevieve Dion. Her research focuses on the development of conductive and electrochemically active fiber and yarn electrodes

using MXene. She has developed various forms of textile energy storage devices that have the potential to power future generations of smart garments. She received her BS in Fiber Science from Cornell University in 2015. She is also a recipient of an Australia–Americas PhD Fellowship, awarded by the Australian Academy of Science.



Jizhen Zhang is a PhD candidate at the Institute for Frontier Materials, Deakin University under the supervision of Prof. Joselito M. Razal. His research interests include the development of fiber-based energy storage devices using 2D materials, with an emphasis on studying large sheets and liquid crystal formulations of $\text{Ti}_3\text{C}_2\text{T}_x$

MXene. He has successfully developed flexible and elastic yarn shaped supercapacitors that demonstrate promise in powering portable electronic devices. He received his BS and MS degrees from Qingdao University in 2012 and 2015, respectively.



Joselito M. Razal is a Professor at the Institute for Frontier Materials and the Deputy Director of the Australian Research Council Research Hub for Future Fibers at Deakin University. His research interest is functional fibers that can be integrated into wearable devices, portable electronics, bioelectronic interfaces,

smart textiles, and wearable energy storage and energy harvesting systems using high aspect ratio MXenes and graphene oxide. He is also involved in scalable manufacturing, working alongside a number of industry partners, to translate bench-scale research into commercial prototypes. He is also a recipient of an ARC Future Fellowship (held at Deakin).

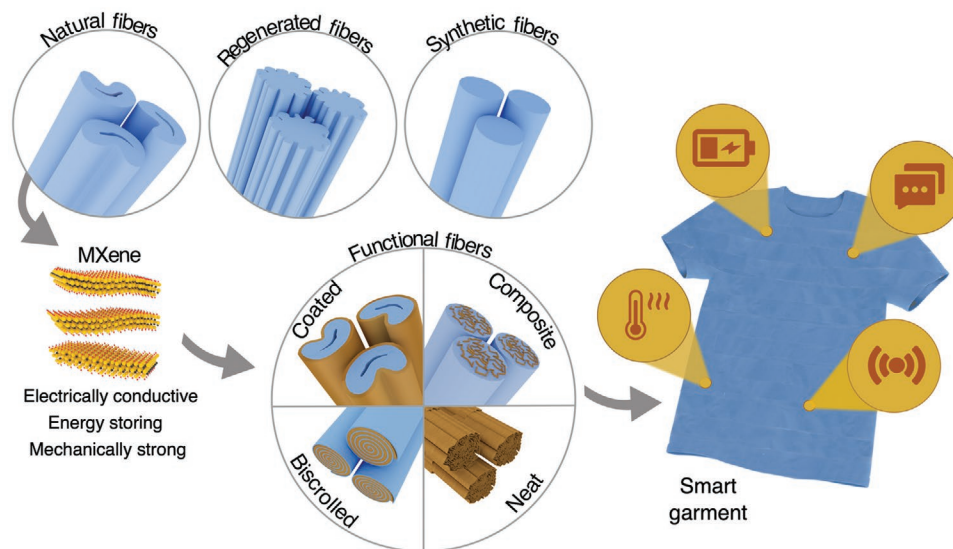


Figure 1. Illustration depicting the development of fibers from natural, regenerated, and synthetic sources to functional fibers to enable smart garments. By incorporating MXenes into fibers, a variety of functional fiber architectures (coated, biscrolled, composite, and neat) can be made. The integration of these fibers into textiles renders the garment “smart” – capable of storing charge, harvesting energy, heating, sensing, and communicating with nearby electronics.

yarns, made by various fabrication techniques, demonstrate a wide range of electrical, mechanical, and electrochemical properties. In this article, we provide an overview of processing single-layer MXene flakes into dispersions, fibers, and yarns, and finally, textile devices. We highlight the fabrication methods used to develop MXene-based fibers, yarns, and fabrics and how these methods influence material properties and device performance. Moreover, challenges relating to the improvement of the mechanical and electrochemical properties of MXene-based fibers are discussed to guide future studies toward their practical application in textile-based devices.

2. MXene Synthesis and Dispersion Preparation

Synthesis and preparation of MXene dispersions are the first steps toward introducing MXenes into fiber/yarn/fabric architectures. With the optimization of MXene synthesis methods, high quality single-layer flakes are now easily achieved. These flakes not only exhibit outstanding electrical conductivity but also possess good dispersibility in a wide range of solvents due to functional groups (T_x) on the surface of MXene flakes.^[35] Initial studies on the rheological properties of aqueous dispersions of MXene showed that these properties are highly dependent on flake size, concentration, and solvent selection. As demonstrated in recent works, tuning the rheological behavior of MXene dispersions allows a wide range of solution processing techniques including spin coating, spray coating, drop-casting, and extrusion printing.^[45–47] Most importantly, the above discoveries and knowledge apply to the fabrication of MXene-based fibers and yarns, including composite fibers and coated yarns. This section details the key parameters involved in the synthesis and preparation of MXene-based dispersions for fiber spinning and coating.

2.1. MXene Synthesis

Since its discovery, a growing number of synthesis methods have been developed to increase the yield of high-quality single-layer MXene flakes. Generally, $Ti_3C_2T_x$ is synthesized by selective wet-chemical etching in hydrofluoric acid (HF)-containing or HF-forming etchants.^[48,49] The first method used to selectively etch aluminum (Al) from Ti_3AlC_2 MAX phase involved exposing the MAX powder to different concentrations of HF solutions.^[21] However, the strong interaction between flakes resulted in multilayer particles with an accordion structure, requiring separate intercalation and delamination processes to produce monolayer MXenes.^[50,51] To improve the yield of monolayer MXenes and simplify the synthesis procedure, new synthesis methods have been developed, such as the minimally intensive layer delamination (MILD) method^[48] and the mixed-acid method.^[45,52] Briefly, the MILD method uses a mixture of lithium fluoride (LiF), hydrochloric acid (HCl), and deionized water as the etching solution. HF is formed when LiF is dissolved in an HCl solution and Li^+ ions work as intercalating agents, leading to Al-free and delaminated MXene in a single step. The delaminated single-layer MXene flakes are readily collected after several washing cycles when the pH of the supernatant approaches ≈ 6 .

Unlike the MILD method, where etching and delamination occur in a single step, the mixed-acid method consists of separate etching and delamination steps. In this method, the etching solution consists of HCl, deionized water, and 49% hydrofluoric acid in a volume ratio of 6:3:1.^[52,53] After etching, the washed sediment is mixed with an intercalating agent (lithium chloride) and delamination occurs after several washing cycles. Extensive research in optimizing both MILD and the mixed-acid method has shown that the precise synthesis conditions, including the etching time and temperature,^[54] and the quality of the MAX phase precursor,^[48,55] influence the yield and the properties of

the resulting MXene dispersion.^[48] Variations in parameters and new synthesis methods have aided in the development of highly concentrated aqueous dispersions of single- to few-layer flakes, up to ≈ 150 mg mL⁻¹,^[56] enabling the fabrication of new architectures such as MXene aerogels^[57] and neat MXene fibers.^[56]

2.2. MXene Flake Size

For 2D materials, which have nanoscale thicknesses, the lateral flake size (defined as the longest dimension of a flake) varies depending on the synthesis conditions and post-processing. The lateral size of flakes plays an important role on the processability of the material into complex structures and the properties of the resulting structures. Using graphene oxide (GO) as an example, it has been shown that flakes can be produced from 100 nm to ≈ 100 μm ,^[58,59] resulting in a variety of rheological^[60,61] and mechanical properties.^[10,62,63] In terms of spinnability, continuous GO fibers can be spun at concentrations as low as 0.75 mg mL⁻¹ when the flake size (measured by its nominal diameter) is large (≈ 37 μm).^[59] However, when the flake size is reduced to ≈ 200 nm, GO is not spinnable even at concentrations as high as 14.6 mg mL⁻¹.^[60] Not only do large flakes aid in the development of fibers, but they have also been shown to improve the mechanical strength and conductivity of the resulting fibers due to a high degree of ordering and a reduced number of defects and edges.^[10]

Likewise, several methods have been reported to control the size and distribution of MXene flakes.^[8,64] For the initial synthesis method using high concentrations of HF, sonication was required to delaminate multilayer MXene, resulting in small flakes (with an average lateral size of ≈ 100 – 300 nm) and narrow size distribution.^[48,65,66] However, for single-layer MXene synthesized by the MILD method or mixed-acid method, flakes show a wide distribution of sizes, from 100 nm to ≈ 10 μm . Using the sucrose density gradient method, small (≈ 130 nm) and large (≈ 4 μm) flakes can be separated by taking advantage of the mass differences between flakes with different lateral sizes.^[64] Another approach to achieve small flakes is to use bath or probe sonication. By tuning the sonication conditions, flakes with varied sizes, ranging from 0.1 to 5 μm , can be obtained with narrow distributions.^[64] Besides the influence of synthesis method, flake size is also related to the size^[56] and the carbon source of the precursor MAX phase.^[55] For example, Ti₃AlC₂ MAX phase synthesized from graphite tends to form larger flakes on average (4.2 μm) compared to those synthesized from carbon lampblack (0.5 μm).^[55]

Control over flake size has allowed researchers to probe single-flake properties, in addition to flake size effects on the properties of assembled MXene-based structures. For the former, large monolayers and bilayers were used to perform nanoindentation studies and the effective Young's modulus of a single-layer of MXene was found to be ≈ 0.33 TPa, which was the highest among the mean values reported in nanoindentation experiments for other solution-processed 2D materials, such as GO.^[67] To study the effects of flake size on properties, single- to few-layer flakes were assembled into films via vacuum-assisted filtration and the electrical and electrochemical

properties of the films were measured as a function of flake size. MXene films produced from small flakes (≈ 130 nm on average) had lower electrical conductivity (≈ 1000 S cm⁻¹) than films produced from larger flakes (≈ 4.4 μm on average, ≈ 5000 S cm⁻¹), likely due to more interfacial resistance and a higher concentration of defects.^[64] However, MXene films composed of ≈ 1.0 μm flakes showed higher capacitance than those composed of ≈ 4.4 μm flakes (288 F g⁻¹ vs 270 F g⁻¹). Films composed of ≈ 0.35 μm flakes showed the best capacitance retention of $\approx 70\%$ when the scan rate increased from 2 to 1000 mV s⁻¹.^[64] The capacitance and rate performance suggested that the transport resistance and ion accessibility of MXene film electrodes were highly dependent on flake size and stacking.^[64] The same effects will be important to consider for MXene-based fiber electrodes.

2.3. Solvent Selection and Stability

Solvent selection is an important factor for spinning fibers, as it can affect the viscosity of the spinning dope, the stability, the spinning method, and the electrical properties of the resulting fibers. Soon after the discovery of Ti₃C₂T_x MXene, MXene-based vacuum-assisted filtered films,^[69] spray-coated films,^[31] and polymer composites,^[70] were processed using aqueous dispersions because the surface terminations (Figure 2a) gave MXene a relatively low zeta potential in the range of -39.5 to -63 mV at neutral pH.^[71,72] However, a wide range of polymers and other materials cannot be dispersed or dissolved in water. To address this issue, the dispersibility of Ti₃C₂T_x in organic solvents was studied using simple solvent exchange processes consisting of repeated centrifugation and manual shaking.^[35,36] As shown in Figure 2b, polar solvents, like dimethylformamide (DMF) and dimethylsulfoxide (DMSO), were identified as better dispersing Ti₃C₂T_x due to somewhat similar polar termination groups, although low concentration dispersions in many other solvents, such as ethanol, can be achieved with sonication and centrifugation.^[35]

Beyond dispersibility, understanding the stability of MXene in both aqueous and organic solvents is important for fiber processing and large-scale applications. It is well-known that aqueous MXene dispersions are sensitive to oxygen-containing environments. For example, it was shown that storage in open vials led to the formation of cloudy-white colloidal suspensions containing primarily anatase titanium dioxide (TiO₂).^[74] To improve their stability, it is recommended to degas the deionized water prior to dispersing MXene sediment to slow oxidation.^[48]

To better understand the flocculation and deflocculation mechanisms, the stability of aqueous MXene dispersions was studied at various pHs and NaCl concentrations.^[75] It was found that the addition of an acid, a base, or a salt to an aqueous dispersion of MXene induced aggregation that led to sedimentation.^[76] With the addition of an acid, complete sedimentation was observed when the pH reached 5 due to the zeta potential moving closer above ≈ -35 mV and decreasing repulsion between the particles.^[77] With the addition of a base, protonation of MXene led to the zeta potential crossing the stable colloidal solution threshold.^[75]

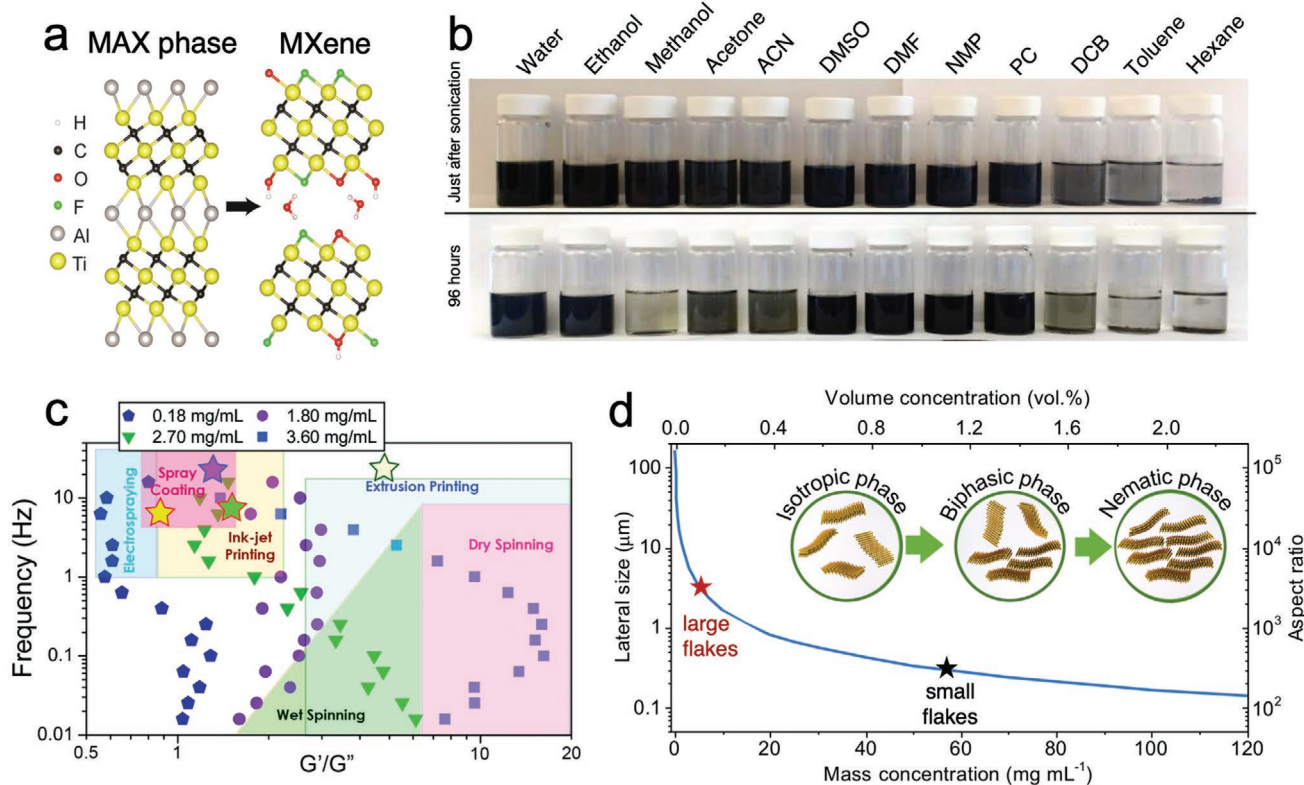


Figure 2. MXene synthesis and dispersion preparation. a) Schematic illustrating the process of removing Al from Ti_3AlC_2 to produce $Ti_3C_2T_x$ MXene. Termination groups (such as $-OH$ and $-F$) are shown on the surface of MXene flakes, along with interlayer water. Adapted with permission.^[73] Copyright 2016, The Royal Society of Chemistry. b) Dispersions of $Ti_3C_2T_x$ flakes in 12 solvents. Adapted with permission.^[35] Copyright 2017, American Chemical Society. c) Frequency dependence of the ratio of G' (the elastic modulus) to G'' (the viscous modulus) for single-layer $Ti_3C_2T_x$ MXene flakes dispersed in water. Reproduced with permission.^[34] Copyright 2018, American Chemical Society. d) Theoretical calculations of the relationship between the lateral size of MXene flakes and the MXene concentration for the isotropic to nematic phase transformation. The red star and black star represent the experimental results for large and small MXene flakes, respectively. Adapted with permission.^[56] Copyright 2020, American Chemical Society.

In addition to the pH and salt concentration, the solvent choice has shown to affect the oxidation stability of MXene in air. In comparison to aqueous dispersions, MXene dispersed in DMF showed improved stability, as evident by a dark supernatant after storage in a laboratory bench for 40 days, likely due to the stabilization solvation shell provided by DMF.^[35,48] However, in terms of electrical conductivity, it has been shown that MXene films prepared from aqueous dispersions have significantly higher conductivity than those prepared from DMF and DMSO.^[41] Depending on the application, the solvent should be carefully selected with stability and electronic properties in mind. From the results of these works, we have a “library” of polar organic solvents to choose from that can disperse MXene, opening new avenues to develop a wide range of MXene composite dispersions for fiber spinning and other processing methods.

2.4. Rheological Properties and Liquid Crystalline Behavior of MXenes

For many fiber fabrication techniques, the rheological properties of the spinning dope or coating formulation play an important role in the ability to form continuous fibers or uniformly

coat fiber substrates, respectively. As demonstrated by rheological studies on GO dispersions, the spinning process highly depends on the viscosity, elastic moduli (G'), viscous moduli (G''), and G'/G'' ratio of dispersions.^[78] Generally, high viscosity with a shear-thinning behavior is required to provide good flowability under shear. Additionally, a high ratio (>1) between G' and G'' ensures that the structure is maintained after the shear force is removed. Tuning these parameters by adjusting the volume fraction (concentration) of GO flakes enabled a wide range of fabrication methods from spray coating to wet spinning.^[78] For MXene, however, the rheological properties have only been reported recently.

The first rheological study on aqueous MXene dispersions revealed that single-layer and multilayer MXenes exhibited different rheological behaviors. For example, a dispersion of single-layer flakes reached a high viscosity at a low concentration of $3.6 mg mL^{-1}$, compared to 70 wt% for multilayer flakes. The high viscosity of MXene dispersions suggested high resistance to flow at low shear rates, which affects the formation of continuous fibers and other solution processing methods.^[46,56] Using a methodology described by Wallace and co-workers,^[78] the ratio of G'/G'' can be plotted as a function of frequency to understand how the rheology of aqueous dispersions of single-layer MXene flakes changes at different

processing rates (Figure 2c).^[34] Noteworthy, although the G'/G'' ratio of single-layer $\text{Ti}_3\text{C}_2\text{T}_x$ at 3.6 mg mL^{-1} is shown to be suitable for dry spinning on the plot, the elastic modulus at this concentration ($\approx 2 \text{ Pa}$) is too low for dry spinning ($>100 \text{ Pa}$).

These properties, G' and G'' , were influenced by both MXene flake size and concentration. MXene dispersions consisting of large flakes (average flake size of $\approx 3.1 \mu\text{m}$) exhibited a high zero-shear (yield) viscosity of $\approx 5050 \text{ Pa s}$ at $\approx 26.5 \text{ mg mL}^{-1}$, which was observed at a much higher concentration for small flakes ($\approx 150 \text{ mg mL}^{-1}$, average size $\approx 310 \text{ nm}$).^[56] Additionally, both dispersions exhibited a strong dominance of G' over G'' throughout the frequency range of 10^{-2} – 10^2 Hz . These results suggested that MXene dispersions consisting of both small and large flakes can exhibit viscoelastic gel-like properties, expanding the opportunities for spinning fibers from a variety of flake sizes. More recently, it was found that aqueous MXene dispersions with average lateral size of $8 \mu\text{m}$ exhibited an elastic modulus of $\approx 36 500 \text{ Pa}$ at a concentration of 50 mg mL^{-1} , reaching the required range for 3D printing.^[46]

In addition to the rheological behavior, the formation of liquid crystals (LCs) and ordered phases are important conditions for spinning pure and continuous fibers consisting of high aspect ratio nanomaterials, such as MXene, GO, and CNTs.^[10,59,79] In 2018, Xia et al.^[57] found LC behavior in a mixture of MXene and CNTs and produced films of vertically aligned flakes by mechanically shearing the mixture. The vertically aligned films showed improved rate performance relative to neat MXene films produced via vacuum-assisted filtration. More recently, LC behavior was found in aqueous and organic dispersions of MXene without additives or binders. According to Onsager theory,^[80] an isotropic dispersion containing randomly oriented flakes can achieve long range orientational ordering and form nematic phases at a critical transition concentration (C_t). The C_t for the isotropic–nematic transition in MXene followed an inverse dependence on flake size (Figure 2d). Aqueous dispersions consisting of small flakes resulted in higher C_t , while dispersions consisting of larger flakes led to lower C_t values. The formation of LC phase for 2D materials is beneficial for self-assembling and aligning flakes during solution processing, which is critical for spinning nanomaterials such as CNT,^[79,81] GO,^[59,61,82] and nanofibers.^[83–85]

3. Fabrication Methods: MXene-Based Fibers, Yarns, and Fabrics

There are two approaches to introduce active materials, including MXene, into textile-based architectures in order to achieve the desired energy storage function. One approach is to coat fibers or yarns, such as cotton, polyester, and nylon, with an electrochemically active material. This approach has been employed with a variety of active materials, including activated carbon,^[8,86] chemically reduced graphene oxide (rGO),^[87–89] and metal oxide particles.^[90,91] Depending on the yarn substrate and the active material, the active material may infiltrate into the yarn, coating individual fibers, or may create a shell around the surface of the yarn. Another approach is to introduce the active material into a spinning formulation and produce

customized composite fibers by melt spinning, wet spinning, electrospinning, or other methods.^[11,92–94] As for MXene-based fibers, owing to the excellent electrical conductivity of MXene and its 2D nature, early works focused on the coating method; introducing MXene into textile architectures by employing an aqueous MXene dispersion as a coating formulation. Recently, different MXene-based fibers, from monofilament fibers to nonwoven mats of fibers, have been achieved using fabrication techniques such as wet spinning, electrospinning, and bicroiling. In this section, details of the existing fiber processes are reviewed in terms of simplicity, scalability, and cost.

3.1. Coating Methods

Coating methods are the simplest and most cost-effective methods to introduce MXenes into textiles. Several coating methods have been explored, including dip coating, spray coating, and drop-casting (Figure 3a). Using these methods, both natural fibers (cotton, linen, and bamboo)^[40,95] and synthetic fibers (nylon,^[96] polyester,^[39] silver-coated nylon,^[37] and carbon-based fabrics^[38,97,98]) have been coated with MXene. Individual fibers, twisted yarns, and knitted and woven fabrics have been used as substrates. Regardless of the method chosen, the first step in coating these materials involves the preparation of a homogenous MXene dispersion, which in all reports, has been an aqueous dispersion. Next, the fiber-based substrate is either sprayed, drop-cast, or soaked with MXene depending on the coating approach. The coated substrates are dried in air or in an oven at low temperatures ($<80 \text{ }^\circ\text{C}$) to quickly evaporate the solvent without oxidizing MXene or burning the fiber substrate. This process can be repeated until the desired MXene loading is achieved.

For example, Hu et al.^[37] used the drop-casting technique to coat silver-plated nylon yarns with MXene. Silver-plated nylon yarns were selected due to their high electrical conductivity and knittability. An aqueous suspension of MXene was loaded dropwise onto pretreated silver-plated nylon fibers that were placed on a hotplate at $50 \text{ }^\circ\text{C}$. After subsequent drops, the MXene loading achieved was $\approx 0.7 \text{ mg cm}^{-1}$. Scanning electron microscope (SEM) images of the pristine and coated silver-plated nylon fibers demonstrated that the MXene flakes coated the surface of individual fibers (Figure 3a-i). The same morphology was seen for MXene-coated carbon fiber fabric (Figure 3a-iii).^[98] When cotton yarn was coated with small flakes, the flakes infiltrated into the yarn and between individual fibers (Figure 3a-iv).^[40] When large flakes were used, they covered the whole bundle of yarn and no infiltration was observed. In another work, MXene flakes were spray-coated layer-by-layer with multiwalled carbon nanotubes (MWCNTs) onto electrospun polycaprolactone (PCL) fiber networks.^[101] The porous PCL network and conductive MWCNT spacer not only limited the restacking of MXene flakes but also increased the accessible surface of the active materials. The fiber electrodes were flexible and foldable, demonstrating good tolerance against repeated mechanical deformation, including twisting and folding.

While the coating process is simple, the surface chemistry and morphology of the fiber-based substrate play a critical role in the adhesion between MXene flakes and individual

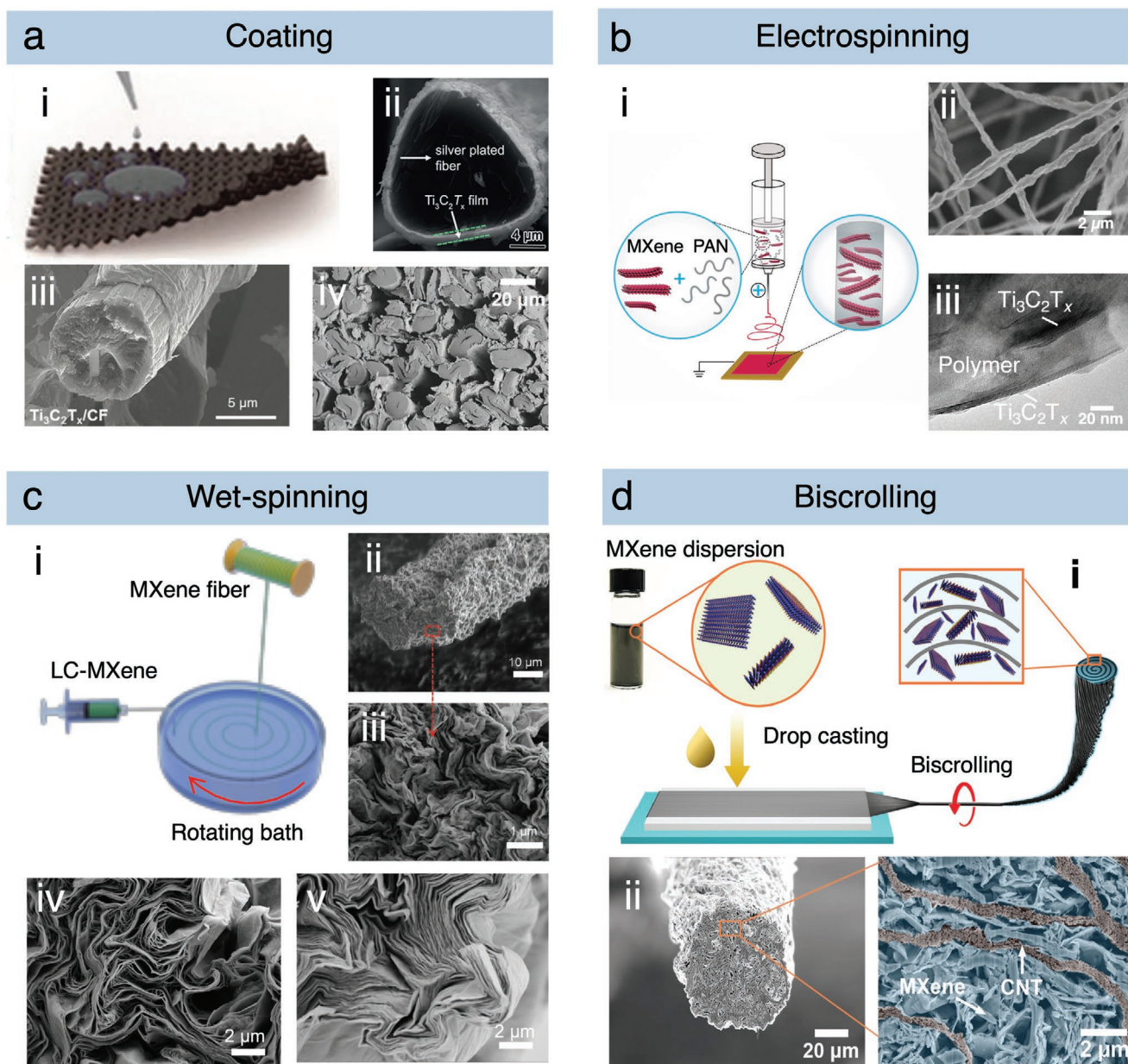


Figure 3. Approaches for producing MXene-based fibers, yarns, and fabrics. a) Coating method: i) schematic representing the fabrication process of MXene coated fabrics. Reproduced with permission.^[98] Copyright 2018, WILEY-VCH; ii) SEM cross-sectional images of $\text{Ti}_3\text{C}_2\text{T}_x$ flakes coated on silver-plated nylon fibers. Reproduced with permission.^[37] Copyright 2017, WILEY-VCH; iii) cross-sectional SEM image of an individual fiber from carbon fabric wrapped with MXene. Reproduced with permission.^[98] Copyright 2018, WILEY-VCH; iv) SEM cross-sectional image of cotton yarn coated with small size MXene flakes. Reproduced with permission.^[40] Copyright 2019, WILEY-VCH. b) Electrospinning method: i) schematic of the production of MXene/PAN nanofibers via electrospinning; ii) SEM images of electrospun PAN fibers with 16 wt% MXene in the electrospinning solution; iii) TEM image of a fiber surface (as-spun) produced from a solution of 10 wt% MXene/8 wt% PAN, showing MXene flakes inside of the fiber. Adapted with permission.^[52] Copyright 2019, The Royal Society of Chemistry. c) Wet spinning method: i) schematic illustration of the custom-built wet spinning setup used to produce neat MXene fibers. Reproduced with permission.^[56] Copyright 2020, American Chemical Society; ii,iii) SEM images of the cross-section of a typical composite fiber with 70 wt% of MXene, 30 wt% PEDOT:PSS at different magnifications. Reproduced with permission.^[99] Copyright 2019, WILEY-VCH; iv,v) cross-sectional SEM images of a neat MXene fiber produced from an acetic acid and chitosan coagulation bath, respectively. Reproduced with permission.^[56] Copyright 2020, American Chemical Society. d) Biscrolling method: i) schematic of the fabrication process for MXene/CNT yarns; ii) SEM image of cross-section morphologies of the composite yarn containing 97.4 wt% MXene at low and high magnifications, respectively. Reproduced with permission.^[100] Copyright 2018, WILEY-VCH.

fibers. $\text{Ti}_3\text{C}_2\text{T}_x$ carries a negative charge due to the polarity of its surface functional groups in aqueous solutions.^[77] As such, it can interact with hydrophilic substrates, positively

charged substrates, and/or substrates containing hydroxyl or amine functional groups. For instance, it was demonstrated that MXene adheres well to cotton fibers, as was evident from

the minimal changes in resistance and MXene mass loading of coated cotton yarns after a series of washing cycles at temperatures up to 80 °C under continuous stirring.^[40] In another work, the interactions between MXene and nylon-6 fibers were studied.^[96] X-ray photoelectron spectroscopy (XPS) results showed an additional peak in the N 1s spectrum in the MXene-coated nylon fibers at ≈397.5 eV, which was assigned to Ti–N bonding. It was speculated that this bond is formed through a dehydration reaction between –OH groups on the surface of MXene and hydrogen atoms from nylon's amide groups. These results indicated that there may be a covalent bond between Ti₃C₂T_x and nylon, suggesting good adhesion between nylon fibers and MXene flakes.

To uniformly coat fiber substrates that cannot readily interact with Ti₃C₂T_x flakes, such as hydrophobic silver-plated nylon fibers, several pretreatments have been explored. These pretreatments included exposure to oxygen plasma, which decorated the surface of fiber substrates with oxygen containing groups. For example, silver-plated nylon fibers were exposed to oxygen plasma for 5 min prior to coating with MXene, rendering them hydrophilic.^[37] Another method to improve adhesion is to mix MXene with conducting polymer binders, which can act as glue to bind MXene to fibers and facilitate adhesion to fiber surfaces. For example, with the aid of PEDOT:PSS, MXene was loaded onto a carbon tow with high mass loadings up to 3 mg cm⁻¹,^[38] which is 5 times higher than a previous report on cotton yarns coated with activated carbon.^[8] To further improve the adhesion of MXene onto hydrophobic substrates, a chemical method to modify the surface chemistry of the substrate may be required. Park et al.^[39] immersed polyethylene terephthalate (PET), cellulose, and nylon threads in 2% v/v 3-aminopropyl triethoxysilane (APTES) and ethanol for 30 min to generate amine (NH₂) groups. After functionalization, yarns were dipped in an aqueous dispersion of MXene for varying durations. XPS confirmed successful electrostatic interactions between the negatively charged surface terminations of MXene and the positively charged APTES-functionalized PET.

3.2. Electrospinning

Electrospinning is a versatile method for producing nanoscale fibers from a polymer or polymer-based composite solution. Electrospun fiber mats have been used extensively as electrodes in battery and supercapacitor applications due to their high specific surface area, which promotes ion adsorption and/or reversible surface redox reactions.^[102] Polymer composite fibers have been spun by adding nanomaterials to the electrospinning solution, including GO,^[103] pseudocapacitive metal oxide particles like MnO₂,^[12] and transition-metal dichalcogenides.^[104] In general, conductive materials are difficult to electrospin because excess charges in the polymer jet dissipate quickly to the collector plate, inducing opposite charges to the collector and resulting in fibers lifting off from the collector.^[104]

A conventional electrospinning setup consists of a syringe filled with a polymer solution capped with a needle tip and a grounded metal collector (Figure 3b-i). A high voltage is applied to the tip of the needle and when the electrostatic force overcomes the surface tension of the solution, a polymer jet is

extruded from the needle tip and fibers are collected across the metal plate. Electrospinning is highly sensitive to agglomeration because the fiber diameter is on the order of several hundreds of nanometers and agglomeration or restacking of particles or flakes in solution may cause beading or inconsistencies in fiber diameter and morphology. Thus, it is critical to achieve stable homogenous solutions for electrospinning, which is essential for large-scale device fabrication.^[52]

Numerous works have been published on electrospun MXene composite nano fibers, including chitosan/Ti₃C₂T_x fibers,^[105] polyethylene oxide (PEO)/Ti₃C₂T_x fibers,^[106,107] polyvinyl alcohol (PVA)/Ti₃C₂T_x fibers,^[106] alginate/Ti₃C₂T_x fibers,^[106] and PAN/Ti₃C₂T_x fibers (Figure 3b-ii).^[52] To spin these composite fibers, MXene was dispersed in a variety of organic solvents, including DMF for spinning PAN, ethanol for spinning PVA, trifluoroacetic acid for spinning chitosan, and water for spinning PEO and alginate-based solutions. These works demonstrated that single- to few-layer flakes and multilayer MXene particles can be trapped within individual nanofibers, as evident by transmission electron microscopy (TEM) images (Figure 3b-iii).^[52,108] This morphology is advantageous for wearable applications because the polymer coating around individual MXene flakes and/or particles may provide protection from abrasion and washing. However, electrospun MXene composite fibers are challenging for direct use as supercapacitor electrodes because flakes are trapped within polymer fibers and surrounded by polymer chains and the MXene loading must be high to render the fibers conductive. Thus, little work has been published on electrospun MXene composite fiber electrodes.^[52,107] One approach explored was to carbonize PAN/MXene fiber mats to create pores in the fibers and improve their conductivity by transforming the polymer into carbon.^[52] In doing so, the carbonization conditions (temperature and duration) needed to be carefully selected to prevent the formation of bulk titanium carbide and TiO₂, while achieving improved conductivity. In another work, PEO/MXene fibers were electrospun around polyester yarn coated with a thin layer of Ni–Cu.^[107] This design made use of a core–shell architecture, in which the core yarn served as the current collector when the yarns were assembled into a symmetric supercapacitor. Doing so relieved the MXene composite fibers from the requirement of high conductivity. The core–shell yarns were flexible, as evident from various bending tests, and the strength of the yarn could be attributed to the polyester core. These reports suggest that in order for electrospinning to become a viable technique for producing MXene-based fiber electrodes for supercapacitor applications, it will be necessary to explore novel electrospinning techniques that result in fibers with higher conductivity and exposed MXene flakes.

3.3. Wet Spinning

Continuous fabrication of fiber electrodes is vital for their integration into textiles and the development of TSCs. Wet spinning is an efficient way to produce long functional fibers, which has been demonstrated by the production of conductive polymer fibers, CNT fibers, and graphene fibers.^[60,79,81,92,109,110] In this method, a spinning solution is injected through a spinneret into a coagulation bath that causes the fiber to coagulate and

then solidify (Figure 3c-i). The fiber is subsequently removed from the bath, dried, and continuously collected onto a winder.

Due to the good dispersibility of MXene in polar solvents, a large range of materials, e.g., PCL,^[36] polyurethane (PU),^[41] PEDOT:PSS (Figure 3c-ii,iii),^[99] and GO,^[111,112] have been added as components to the spinning dope to produce MXene-based composite fibers. These spinnable materials significantly improved the processability of MXene flakes into fibers. The loading of MXene in those fibers covered a wide range from 10 to 98 wt%.^[111,112] Depending on the components and solution properties of the composite spinning formulations, modifications in the spinning setup, coagulation bath, and post-treatments were required. For instance, spinning MXene/PEDOT:PSS fibers into a sulfuric acid bath required the spinning dope to be injected upward because of its lower density compared to the bath (Figure 3c-i).^[99] As another example, MXene/GO fibers required a chemical reduction process after spinning to reduce the GO and recover the electrical conductivity.^[111,112] One option to simplify the spinning conditions for MXene-based fibers is to directly spin from pure MXene dispersions.

Compared with graphene or GO, MXenes share many similar properties, including liquid crystalline behavior, pseudoplastic rheological properties, and dispersibility in various solvents, and these properties enable the production of neat MXene fibers via wet spinning. It was recently reported that the nematic phase of MXene formed at concentrations of ≈ 26 and 125 mg mL^{-1} for large and small flakes in aqueous solutions, respectively. The extrusion process during fiber spinning applied a shear force to the nematic phase of the LC MXene dispersions, which improved the orientation of MXene flakes along the fiber axis. It was found that the solvent exchange rate between the extruded fiber and the coagulation bath affected the microstructure of the resulting neat MXene fibers. A pure acetic acid coagulation bath had a fast solvent exchange rate with an aqueous MXene dispersion, resulting in fibers with an open microstructure, large diameters and low densities (Figure 3c-iv). A bath consisting of a chitosan dispersion slowed the solvent exchange rate, leading to close-packed MXene fibers (Figure 3c-v). The spinning of pure MXene fibers is a milestone for building MXene-based macroscale architectures.

3.4. Biscrolling

Biscrolling is a fabrication technique that uses drawable CNT sheets as a host to turn nanomaterials, which are often unspinnable, into CNT-supported yarns. This process involves introducing a guest material onto drawn CNT sheets by drop-casting,^[113,114] in situ deposition,^[115] or dip coating^[97] prior to inserting a twist. This method has been used to produce biscrolled CNT hybrid yarns with up to 98 wt% loading of nanoparticles.^[113] The particles are trapped within scroll corridors of the CNT host, but remain electrochemically accessible because of the small diameter and open microstructure of CNT yarns. Biscrolled yarns have found applications as superconductors, electrodes for batteries, supercapacitors, fuel cells, and artificial muscles.^[97,108,114]

To introduce MXene into biscrolled CNT yarns, dispersions of MXene in DMF ($2\text{--}30 \text{ mg mL}^{-1}$) were drop-cast onto stacks of CNT forests and subsequently twisted into a yarn (Figure 3d-i).^[100] SEM images (Figure 3d-ii) revealed that MXene flakes were trapped within helical yarn corridors, creating voids of varying sizes to infiltrate aqueous electrolytes. This method is ideal for achieving high mass loadings of active material, approaching pure MXene fibers. But, the clear shortcomings are the limited length of yarns and the high cost of the CNT forests. Also, the biosafety regarding the use of CNTs in wearable textiles may raise concerns.^[116,117]

4. Electrode Properties and Device Performance

There are a number of property requirements for fiber electrodes in textile-based energy storage devices. The primary function of a fiber electrode is the ability to store charge, which can be made possible through high porosity, open surfaces, and the ability to undergo redox reactions and/or intercalate ions. Another critical demand is high electrical conductivity, which enables electron transfer and decreases the energy loss (voltage drop) inside the device, providing good rate performance. Additionally, high strength and flexibility are required to integrate fiber- or yarn-based electrodes or devices into textiles using a variety of textile manufacturing processes (knitting, weaving, etc.). To date, most of the work on MXene-based fiber electrodes has primarily focused on characterizing electrical, electrochemical, and mechanical properties. **Table 1** details these properties of the MXene-based fibers and yarns described in Section 3. Depending on the MXene content (for spun fibers) or loading (for coated fibers), flake size, and host material (spun fibers), these fibers exhibited a wide range of conductivity values from $\approx 20 \text{ S cm}^{-1}$ for composite fibers^[111] to $\approx 7750 \text{ S cm}^{-1}$ for neat MXene fibers,^[56] tensile strength from $\approx 18 \text{ MPa}$ for neat MXene fibers^[56] to 265 MPa for 54 wt% MXene biscrolled yarns,^[100] and strain-to-failure, from $\approx 1\%$ for neat MXene fibers to $\approx 15\%$ for $\approx 97 \text{ wt\%}$ MXene biscrolled yarns.^[100] Additionally, the capacitance has reached as high as $\approx 700 \text{ mF cm}^{-1}$ for MXene-coated yarns^[40] and 1265 F cm^{-3} for neat MXene fibers in $1 \text{ M H}_2\text{SO}_4$, the latter approaching the volumetric capacitance of MXene films produced via vacuum-assisted filtration. The following section will discuss the factors affecting these properties of fibers and will detail the assembly and performance of TSCs.

4.1. Mechanical Properties

The mechanical properties of a single MXene flake are the highest among the mean values reported from nanoindentation experiments for solution-processable 2D materials.^[67] Namely, the effective Young's modulus reported for $\text{Ti}_3\text{C}_2\text{T}_x$ MXene was $0.33 \pm 0.03 \text{ TPa}$, compared to $0.21 \pm 0.02 \text{ TPa}$ for GO and $0.25 \pm 0.15 \text{ TPa}$ for rGO.^[67] Prior to studying the mechanical properties of MXene-based fibers, MXene was introduced into polymer composite films and the effect of MXene concentration on tensile strength and modulus was studied.^[70] It was found that by introducing MXene into polymer matrices, the

Table 1. Literature review of the electrical, mechanical, and electrochemical properties of MXene-based fibers, yarns, and fabrics. PEDOT:PSS: poly(3,4-ethylenedioxythiophene):polystyrene sulfonate, rGO: reduced graphene oxide, CNT: carbon nanotube, PCL: polycaprolactone, PET: polyester, C_v : volumetric capacitance, C_a : areal capacitance, C_g : gravimetric capacitance, C_L : length-specific capacitance.

Electrode type	Electrode	Active material	Fabrication method	Electrical data		Mechanical data		Electrochemical data					Ref.	
				Conductivity [$S\ cm^{-1}$]	Diameter [μm]	Tensile strength [MPa]	Strain-to-failure [%]	Electrolyte	Electrode length [cm]	C_v [$F\ cm^{-3}$]	C_a [$mF\ cm^{-2}$]	C_g [$F\ g^{-1}$]		C_L [$mF\ cm^{-1}$]
Fiber-based electrode	MXene/PEDOT:PSS fiber	MXene, PEDOT:PSS (70 wt% MXene)	Wet spinning	1489	22	58.7	<2	1 M H_2SO_4	0.5	615	676	258	4.6	[99]
	MXene/rGO fiber	MXene, rGO (88 wt% MXene)	Wet spinning	72.3	70	132.5	2.9	1 M H_2SO_4	1.0	341	233	257	≈ 1.2	[111]
	MXene/rGO fiber	MXene, rGO (90 wt% MXene)	Wet spinning	290	25.4	12.9	≈ 3.75	1 M H_2SO_4	N/A	891	565	495	N/A	[112]
	Neat MXene fiber	MXene (100 wt%)	Wet spinning	7748	46	40.5	1.7	1 M H_2SO_4	0.5	1265	1762	393	N/A	[56]
	MXene/carbon fiber mat	MXene, carbon (≈ 22 wt% MXene)	Electrospinning	N/A	N/A	N/A	N/A	1 M H_2SO_4	N/A	N/A	244	≈ 110	N/A	[52]
	MXene/CNT@PCL fiber mat	MXene, CNT (21.5 wt% MXene/CNT)	Electrospinning	N/A	N/A	3	≈ 97	1 M H_2SO_4	N/A	N/A	≈ 50	≈ 100	N/A	[101]
Yarn-based electrode	Biscrolled MXene/CNT yarn	MXene, CNT (≈ 97 wt% MXene)	Biscrolling	N/A	120	26.6	≈ 15	3 M H_2SO_4	1.0–1.5	1083	3188	523	118	[100]
	Biscrolled MXene/CNT yarn	MXene, CNT (95 wt% MXene)	Biscrolling	2.7	56	38.4	≈ 4.7	6 M LiCl	N/A	92	N/A	N/A	N/A	[118]
	MXene/PEDOT:PSS-coated carbon tow	MXene, PEDOT:PSS (1.8 mg cm^{-1} MXene)	Coating	≈ 198	120	≈ 3000	≈ 1.6	PVA/ H_3PO_4 gel	3.0	N/A	659	30.8	252.6	[38]
	MXene/silver-coated nylon yarn	MXene (0.7 mg cm^{-1})	Coating	N/A	500	N/A	N/A	PVA/ H_2SO_4 gel	N/A	N/A	328	N/A	50	[37]
	MXene-coated cotton yarn	MXene (78 wt%)	Coating	199	610	460	10	1 M H_2SO_4	2.5–3.0	0.26	3965	N/A	760	[40]
	MXene/PET/silver-coated nylon yarn	MXene (N/A)	Electrospinning	N/A	N/A	N/A	N/A	PVA/ H_2SO_4 gel	2.0	N/A	72	N/A	N/A	[107]
Fabric-based electrode	MXene-coated carbonized silk fabric	MXene (2 mg cm^{-2})	Coating	N/A	N/A	N/A	N/A	1 M H_2SO_4	N/A	N/A	362	N/A	N/A	[68]
	MXene-coated carbon fiber fabric	MXene (2.6 mg cm^{-2})	Coating	N/A	N/A	N/A	N/A	1 M H_2SO_4	N/A	N/A	416	200	N/A	[98]
	MXene-coated cotton knit fabric	MXene (≈ 22.5 mg cm^{-2})	Coating, knitted	N/A	N/A	N/A	N/A	1 M H_3PO_4	≈ 0.5	N/A	707	31	566	[96]

tensile strength and Young's modulus of composite films were enhanced relative to pure MXene or pure polymer films.^[70] For example, by adding 40 wt% MXene to PVA, the tensile strength and modulus increased from 30 ± 5 MPa and $1.0 \pm$

0.3 GPa for pure PVA films, respectively, to 91 ± 10 MPa and 3.1 ± 0.2 GPa for composite films, respectively.^[70] These results suggest great potential for MXene to improve the mechanical properties of fiber architectures.

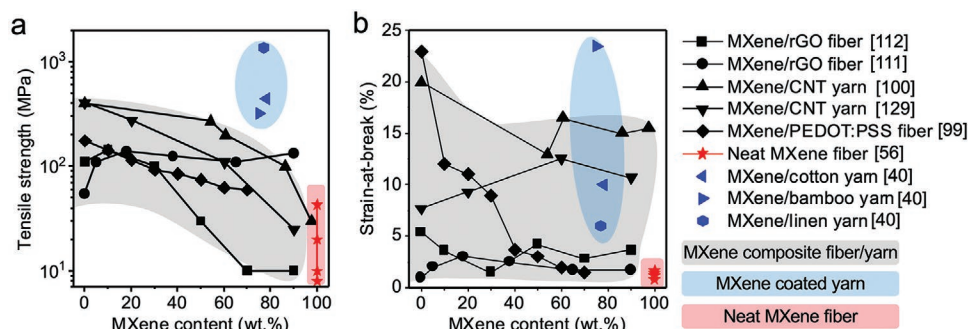


Figure 4. Mechanical properties of MXene-based fibers and yarns. a) Tensile strength as a function of MXene content for MXene-based fibers and yarns, b) strain-at-break as a function of MXene content for MXene-based fibers and yarns.

The mechanical properties of MXene-based fibers are diverse and depend heavily on their composition, structure, and fabrication methods. As shown in **Figure 4a**, the tensile strength of MXene-based fibers ranges from ≈ 10 to ≈ 1370 MPa, with the highest being for coated fibers, followed by composite wet-spun fibers and bistrilled yarns, and ending with neat MXene fibers. MXene-coated fibers exhibited the highest tensile strength due to the high tensile strength of the fiber substrate, in addition to the reinforcement provided by MXene. For example, prior to coating with MXene, pristine cotton yarns had a tensile strength of ≈ 334 MPa and after coating (at 2 mg cm^{-1} loading, ≈ 79 wt% of MXene), the tensile strength increased to ≈ 468 MPa.^[40] Similar trends were reported for MXene-coated linen and bamboo yarns.^[40]

While coated fibers receive support from the fiber substrate, MXene composite fibers have demonstrated improved tensile strength due to the inherent mechanical properties of the host material and the interactions between the host and MXene flakes. For example, adding 50 wt% rGO to an aqueous MXene spinning dope resulted in fibers with a tensile strength of ≈ 34 MPa, almost double that of neat MXene fibers made from small-size flakes.^[112] Similarly, adding 30 wt% PEDOT:PSS to an aqueous MXene spinning dope resulted in fibers with a tensile strength of ≈ 58 MPa.^[119] However, at low loading of host material (≈ 10 wt%), the mechanical strength decreased to ≈ 13 MPa for MXene/rGO fibers^[112] and the same trend was seen for MXene/PEDOT:PSS fibers.^[119] These works demonstrate that the tensile strength improved with the addition of low concentrations of MXene (Figure 4a), while further modifications will be needed to enhance the strength of fibers consisting of high MXene loadings. Improving bonding between MXene flakes and the host material, such as a polymer, is key to achieving good load transfer and high mechanical properties of MXene-based composite fibers.

For pure MXene fibers, the tensile strength ranged from 10 to 40 MPa, depending on the spinning coagulation bath and MXene flake size. Unlike coated fibers, which receive strength from the substrate, and composite fibers, which rely on the interactions between the host material and MXene flakes, neat wet-spun fibers made from MXene and other 2D materials rely on the mechanical properties of individual flakes, their interactions (the weak spot), and their packing density.^[10,59,120–122] Initial work on neat MXene wet-spun fibers showed that these fibers had significantly lower mechanical properties than

individual flakes but surpassed those of MXene freestanding films (≈ 20 MPa).^[70] It was found that increasing the size of flakes resulted in improved tensile strength (≈ 18 MPa for fibers made from small flakes vs 41 MPa for fibers made from large flakes) with little change in strain-to-failure (≈ 1 – 2% for both fibers).^[56]

In terms of the strain-to-failure of composite fibers, for all of the composite fibers tested, the strain-to-failure decreased as a function of MXene loading (Figure 4b). For example, the strain-to-failure decreased from $\approx 5.5\%$ for rGO fibers to $\approx 3.6\%$ for 90 wt% MXene/rGO fibers,^[112] and more notably from 20.1% to 1.1% for pure PEDOT:PSS fibers and 70 wt% MXene/PEDOT:PSS fibers,^[119] respectively. In general, the failure strain of fibers containing high MXene loadings (>70 wt%) is less than 5%. Despite these values, most works have demonstrated that the fibers can resist bending and form tight knots.

The Young's modulus is another important mechanical property to consider during fiber fabrication and development because it relates to the fiber's ability to resist elastic deformation.^[122] The Young's modulus for both composite fibers, MXene/rGO and MXene/PEDOT:PSS fibers, increased as a function of MXene loading. MXene/rGO wet-spun fibers increased from ≈ 7 GPa for pure rGO fibers to ≈ 13.3 GPa for 88 wt% MXene/rGO fibers.^[111] Similarly, the Young's modulus increased from 5.3 GPa for pure PEDOT:PSS to 7.5 GPa for 70 wt% MXene/PEDOT:PSS fibers.^[119] These results indicate that MXene has a significant reinforcement effect on composite fibers.

Like coated and composite wet-spun yarns, which rely on reinforcement from a commercial fiber and host material, respectively, bistrilled yarns receive strength from long CNT yarns, which have a high tensile strength of ≈ 380 MPa.^[100] When MXene was incorporated into bistrilled yarns, the breaking strength decreased as a function of MXene loading from 265 MPa at 54 wt% to 27 MPa for ≈ 98 wt% bistrilled MXene yarns.^[100] At 54 wt% MXene, bistrilled MXene/CNT yarns demonstrated the highest tensile strength for the reported MXene-based fibers at this high loading. The strain-to-failure slightly decreased with the addition of MXene, from $\approx 20\%$ for neat CNT yarns to $\approx 15\%$ for ≈ 98 wt% bistrilled MXene/CNT yarns, however, the strain-to-failure was relatively unchanged between 54 and 97.5 wt% MXene. From these results, it is clear that CNTs provide a strong and flexible backbone for MXene flakes, resulting in a mechanically strong and flexible yarn after drawing and twisting.

4.2. Electrical Properties

One of the most notable properties of $\text{Ti}_3\text{C}_2\text{T}_x$ is its excellent electrical conductivity, which is the highest among solution-processable 2D materials.^[123] Taking advantage of this property, many works have demonstrated that adding MXene into fibers significantly improves their conductivity, as shown in **Figure 5**.

Wet-spun neat MXene fibers achieved the highest conductivity to date, reaching up to 7748 S cm^{-1} (normalized by fiber cross-sectional area determined from SEM).^[56] It was found that the conductivity of neat MXene fibers was greatly affected by flake size.^[56] For instance, the conductivity for neat MXene fibers made from small flakes using a chitosan-based coagulation bath was 3512 S cm^{-1} , which is about half of that of fibers made from large flakes using the same coagulation bath. Additionally, the slow coagulation rate in chitosan increased the stacking of flakes compared with fast coagulation rate in acetic acid, which also contributed to the conductivity enhancement. These densified fibers were approaching the highest reported conductivity of MXene thin films, $\approx 15\,000 \text{ S cm}^{-1}$,^[29] and surpassed that of graphene films and carbon fibers.^[120,124,125]

For most composite fibers, increasing the MXene loading resulted in improved electrical conductivity. For example, the electrical conductivity increased from ≈ 29 to $\approx 72 \text{ S cm}^{-1}$ when 88 wt% MXene was added to rGO fibers, after chemical reduction.^[111] Another factor that affects the conductivity of MXene composite fibers is the solvent used in the spinning formulation. In the case of wet-spun MXene/PU composite fibers, DMSO was used as the solvent to disperse MXene and PU.^[41] The electrical conductivity of 80 wt% MXene/PU fiber was $\approx 155 \text{ S cm}^{-1}$ and 100 wt% MXene fiber was $\approx 392 \text{ S cm}^{-1}$, which is significantly lower than fibers spun from aqueous MXene dispersions. The difference in conductivity is likely due to the enlarged interlayer spacing of MXene in organic solvents relative to that of MXene in water.^[36]

MXene-coated fibers have also exhibited excellent electronic conductivity. The highest reported MXene loading was 79 wt% on cotton, linen, and bamboo fibers.^[40] At this loading, the conductivity reached 200 S cm^{-1} for cotton fibers and 440 S cm^{-1} for linen fibers. The difference in conductivity was attributed to the diameters of the yarns. Linen yarn was significantly finer than the cotton yarn chosen in this work. By increasing

the MXene loading on cotton yarn from 0.6 to 2.0 mg cm^{-1} , the conductivity increased from ≈ 30 – 50 to 200 S cm^{-1} . Similarly, by increasing the flake size from an average of 340 nm to $1 \mu\text{m}$ at 0.6 mg cm^{-1} MXene loading, the conductivity increased from ≈ 30 – 50 to 60 – 85 S cm^{-1} .^[40] As was demonstrated with neat MXene fibers, large flakes led to the highest conductivity.

While increasing the MXene loading on coated yarns and wet spun fibers resulted in improvements in conductivity, the opposite effect was observed in bistrilled yarns. For bistrilled yarns, the yarn diameter increased as a function of MXene loading, likely resulting in changes in the packing of MXene flakes and decreasing conductivity. For example, the yarn diameter increased from $42 \mu\text{m}$ for pure bistrilled CNT yarns to $120 \mu\text{m}$ for $\approx 97 \text{ wt}\%$ MXene bistrilled yarns.^[100] As such, the conductivity decreased from 235 to $\approx 25 \text{ S cm}^{-1}$.

4.3. Electrochemical Properties of Fiber Electrodes

The high volumetric capacitance of $\text{Ti}_3\text{C}_2\text{T}_x$ makes it a promising candidate for fiber-based electrodes with excellent electrochemical performance.^[25,57,65] Prior to the development of MXene-based fiber electrodes, the effects of many factors, including flake size, orientation, density, and concentration, on the electrochemical performance of neat MXene films and MXene composite films were studied.^[25,57,126,127] These factors have also played a significant role on the electrochemical performance of MXene-based fibers, in addition to fiber structure (e.g., loading of MXene and packing density of fibers) and electrochemical system design (e.g., the electrolyte, fiber composition, and counter electrodes).

For MXene-coated yarn electrodes, MXene acts as the main active material and current collector determining their electrochemical performance. The capacitance of MXene-coated yarns increases with MXene loading. While the length-specific capacitance of MXene-coated fibers is high (up to $\approx 760 \text{ mF cm}^{-1}$ for MXene-coated cotton yarns tested in $1 \text{ M H}_2\text{SO}_4$),^[40] the volumetric capacitance is often modest due to the large volume occupied by the yarn substrate. For instance, the volumetric capacitance of MXene-coated cotton yarns was 260 F cm^{-3} in $1 \text{ M H}_2\text{SO}_4$,^[40] compared to 1500 F cm^{-3} for MXene films.^[25] However, the volumetric capacitance of MXene-coated yarn still exceeds that of carbon-coated yarn electrodes.^[8,128]

MXene-based composite fibers have two main advantages over MXene-coated fibers in terms of electrochemical performance. First, the volume is easily tuned, meaning that fine fibers can be produced, leading to high volumetric capacitances. Second, high MXene loadings can be achieved ($>80 \text{ wt}\%$, the highest MXene loading achieved on coated fibers).^[40] As demonstrated by the production of wet-spun MXene/rGO fibers,^[111,112] a MXene loading of $\approx 88 \text{ wt}\%$ was achieved for fibers with diameters in the range of 30 – $50 \mu\text{m}$. These fibers exhibited a volumetric capacitance of $\approx 341 \text{ F cm}^{-3}$ in H_2SO_4 at 0.5 A cm^{-3} .^[111] Similarly, bistrilled MXene/CNT yarns with a MXene loading of $\approx 98 \text{ wt}\%$ (fiber diameter: $\approx 120 \mu\text{m}$) displayed record specific volumetric, aerial, gravimetric, and linear capacitance values of 1083 F cm^{-3} , 3188 mF cm^{-2} , 428 F g^{-1} , and 118 mF cm^{-1} , respectively, at a current density of 2 mA cm^{-2} in $3 \text{ M H}_2\text{SO}_4$ electrolyte.^[100] Neat MXene fiber reached the highest volumetric capacitance of 1265 F cm^{-3} .

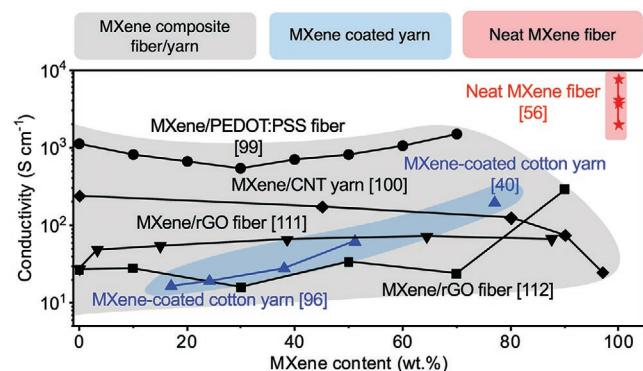


Figure 5. Electrical conductivity of MXene-based fibers and yarns. The electrical conductivity of MXene-based fibers and yarns as a function of MXene content.

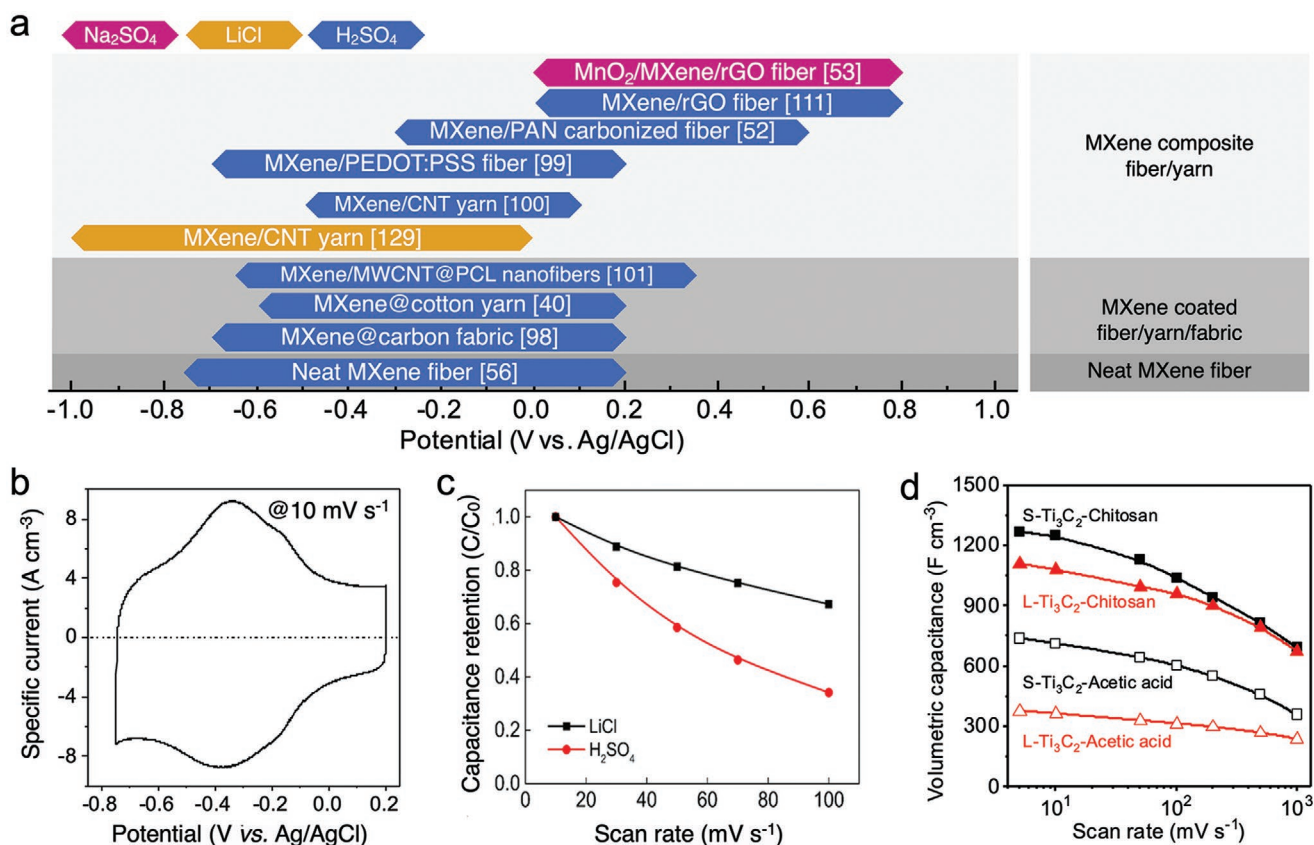


Figure 6. The electrochemical properties of MXene-based fibers, yarns, and fabrics in three-electrode setups. a) The operation window of MXene-based fibers in various electrolytes versus Ag/AgCl. b) A representative cyclic voltammogram (CV) of a neat MXene fiber tested in 1 M H₂SO₄ (300 nm average flake size, chitosan coagulation bath). Adapted with permission.^[56] Copyright 2020, American Chemical Society. c) Capacitance retention of a bisrolled MXene/CNT fiber in different electrolytes while the scan rate increased from 10 to 100 mV s⁻¹. Capacitance values were normalized by the capacitances in each electrolyte at the lowest scan rate. Reproduced with permission.^[129] Copyright 2019, Materials Research Society. d) The rate performance of neat MXene fibers produced from large (L-Ti₃C₂) and small (S-Ti₃C₂) flakes in acetic acid and chitosan coagulation baths. Reproduced with permission.^[56] Copyright 2020, American Chemical Society.

The study of neat MXene fibers also revealed the effects of MXene flake size and fiber morphology (packing density) on energy storage performance (in addition to the electrical conductivity mentioned above). For example, neat MXene fibers made from small flakes exhibited higher volumetric capacitance than those made from large flakes, as a result of a large number of defects and edges on small Ti₃C₂T_x flakes that improve permeability and ion transport.^[127] Additionally, the volumetric capacitance of fibers produced from a chitosan-based coagulation bath (SCH fiber) was higher than those produced using an acetic acid bath (SAA fiber). The volumetric capacitance of SCH fiber (≈1265 F cm⁻³) was ≈2 times higher than that of SAA fiber (≈737 F cm⁻³). The difference in volumetric capacitance can be attributed to the higher density of the SCH fibers (≈3.6 g cm⁻³) compared to that of SAA fibers (≈1.7 g cm⁻³). Although the density of the obtained SCH fibers was significantly lower than MXene films with close stacked flakes (>3.8 g cm⁻³),^[65] the volumetric capacitance of SCH fiber was comparable to the reported highest value of pure MXene film (≈1500 F cm⁻³).^[25]

Another factor that affects the capacitance of MXene-based fiber electrodes is the potential window, summarized in

Figure 6a. Neat MXene films operate in a potential window of -1.1 to -0.1 V versus Hg/Hg₂SO₄ (-0.7 to 0.3 V vs Ag/AgCl) in a three-electrode setup, using glassy carbon as a current collector and overcapacitive activated carbon as a counter electrode.^[25] Neat MXene fibers and MXene/PEDOT:PSS composite fibers operate in a similar window, from -0.75 to 0.2 V versus Ag/AgCl (Figure 6b).^[56,99] Generally, the redox peak of MXene in H₂SO₄ electrolyte occurs at -0.75 V versus Hg/Hg₂SO₄ at 100 mV s⁻¹, resulting in high capacitive performance.^[25] However, the operation potential window changes when different electrolytes are used. For instance, MXene/CNT yarn safely reached -1 V (vs Ag/AgCl) in LiCl electrolyte,^[129] while it was limited to -0.55 V (vs Ag/AgCl) in H₂SO₄ electrolyte.^[100] The limited potential window in H₂SO₄ electrolyte compared to that of neat MXene films and fibers was likely due to defects in the MXene and metal impurities in CNTs, which acted as catalysts for hydrogen evolution reactions at low pH values. For MXene/CNT yarn, the Li⁺ ion intercalation process allowed the yarn to better maintain the capacitance at high discharge rates (Figure 6c).^[129]

Moreover, the operation window of MXene-based electrodes was influenced by heat treatment and fiber composition.

For instance, MXene/rGO fibers and MXene/PAN nanofibers carbonized at 600 °C operated in a higher potential window, from 0 to 0.8 V versus Ag/AgCl and from -0.3 to 0.6 V versus Ag/AgCl, respectively.^[52,111] It is deduced that for MXene/rGO fibers with low MXene content, large rGO flakes limited access of ions to small MXene flakes. For MXene/PAN nanofibers carbonized at 600 °C, carbon limited access of ions to MXene flakes. In another case, MnO₂ particles were deposited onto MXene/rGO fibers, but the resulting composite fibers were not stable in acidic electrolyte. Instead, the fibers were tested in Na₂SO₄ and the operation window was from 0 to 0.8 V versus Ag/AgCl, which was the same window used for MXene/rGO fibers in 1 M H₂SO₄. The addition of MnO₂ contributed to a high volumetric capacitance (851 F cm⁻³) in Na₂SO₄ electrolyte, while MXene/rGO fiber showed a volumetric capacitance of 129 F cm⁻³.^[53]

Along with the capacitance, the rate performance of fiber electrodes is an important performance evaluation criterion. The capacitance of MXene-based fibers is attributed to the two fundamental electrochemical processes occurring at the interface between the electrochemical electrode and the electrolyte, namely: i) nondiffusion-controlled pseudocapacitance related to fast Faradaic charge-transfer process with surface atoms and non-Faradaic contribution from the double layer adsorption of ions, and ii) diffusion-controlled Faradaic intercalation processes. The measured current *i* from cyclic voltammogram curves obeys power law relationship with scan rate (*v*), $i = ab^v$ where “*a*” and “*b*” are adjustable parameters. For diffusion-controlled processes, the current response is proportional to the square root of the scan rate ($b = 0.5$); while the current response is proportional to the scan rate ($b = 1$) for capacitive processes. For MXene-based yarns, *b* values obtained at different potentials were in the range of 0.85–1, indicating that the current response is mainly pseudocapacitive in both H₂SO₄ and LiCl electrolytes.^[52,98,129] In this case, the capacitance of electrodes is affected by the size of the ions, whereby smaller ions lead to higher energy density.^[130]

The rate performance of MXene-based fibers is also influenced by their electrical conductivity. Generally, the high loading of MXene gives high capacitance at slow scan rates (2–5 mV s⁻¹); however, the capacitance values were halved when the scan rate was increased to 100 mV s⁻¹ for most MXene-based fibers and yarns.^[38,101,118] For example, the capacitance of MXene/rGO fibers at a scan rate of 100 mV s⁻¹ is only ≈492 F cm⁻³ compared to 890.7 F cm⁻³ at 10 mV s⁻¹. This difference has been attributed to the low electrical conductivity (<300 S cm⁻¹) and ionic transport obstacles created by large rGO sheets.^[112] However, the volumetric capacitance of MXene/PEDOT:PSS composite fibers (70 wt% MXene, 30 wt% PEDOT:PSS) only slightly decreased from 614.5 to 500.3 F cm⁻³ (81.4%) when the scan rate increased from 5 to 200 mV s⁻¹ and over half of the capacitance (375.2 F cm⁻³) was maintained at 1000 mV s⁻¹.^[99] The excellent rate performance can be attributed to the high electrical conductivity of MXene/PEDOT fibers (≈1489 S cm⁻¹). Excellent rate performance was also achieved for neat MXene fibers. As shown in Figure 6d, the a neat MXene fiber made from small flakes (S-Ti₃C₂) showed high capacitance of 1265 F cm⁻³ at 5 mV s⁻¹ and 692 F cm⁻³ at 1000 mV s⁻¹.^[56]

4.4. The Performance of Textile Supercapacitors

Fiber/yarn electrodes are typically fabricated into textile supercapacitor devices using a solid-state electrolyte following various designs including parallel,^[37,107,111,112,118] twisted,^[53,100] face-to-face,^[38] and knitted^[96] configurations (Figure 7). Generally, single fiber electrodes with high capacitance resulted in supercapacitor devices with high energy storage performance. Additional criteria to evaluate the performance of TSCs are the energy density (*E*) and power density (*P*), which depend on the capacitance (*C*), working voltage window (*V*), and internal resistance (*R_s*), which can be expressed by the following equations: $E = \frac{1}{2}CV^2$, and $P = V^2/4R_s$, respectively.

Symmetric TSCs (where the same kind of fiber electrode is used as both anode and cathode) have been well studied using MXene coated fibers,^[37,38] composite fibers,^[99,111,112] and coated fabrics.^[52,101] Symmetric devices have several advantages over asymmetric devices: i) the capacitance of the electrodes is easily matched by using fibers/yarns with the same length or fabrics with the same area, ii) the capacitance is proportional to that of single fiber electrodes, i.e., the higher the electrode capacitance, the higher the capacitance of the assembled device. Taking MXene-coated carbon fiber yarns as an example, the length-specific capacitance increased linearly from ≈25.8 to ≈131.7 mF cm⁻¹ in H₃PO₄/PVA gel electrolyte at 0.2 mA cm⁻¹ when the mass loading of the coating formula (MXene and PEDOT:PSS) increased from 0.4 to 2.0 mg cm⁻¹.^[38] Due to the same characteristic of two electrodes, they share the same operation window. However, the voltage window of symmetric MXene-based supercapacitors is limited to 0.6 V, which is lower than that of carbon-based symmetric supercapacitors (1 V) that use aqueous electrolytes.

To achieve higher energy densities and power densities, asymmetric devices were produced using MXene-based fibers as cathodes. Common counter electrodes for MXene-based electrodes include GO and RuO₂ because they can operate at high positive potentials.^[131–134] For example, asymmetric TSCs were fabricated by pairing bisrolled MXene/CNT yarns with bisrolled RuO₂/CNT yarns (Figure 8a). In doing so, the operation window was extended from 0.6 to 1.6 V in H₂SO₄/PVA gel electrolyte (Figure 8b) and the maximum energy and power density achieved was 61.6 mWh cm⁻³ (168 μWh cm⁻² and 8.4 μWh cm⁻¹) and 5428 mW cm⁻³ (14.8 mW cm⁻² and 741 μW cm⁻¹), respectively.^[100] Additionally, the devices displayed high capacitance retention after repeated bending. A textile-based asymmetric device was also prepared using carbon fabrics coated with MXene and RuO₂ (Figure 8c), which delivered an energy density of 37 μWh cm⁻² at a power density of 40 mW cm⁻², with 86% capacitance retention after 20 000 charge–discharge cycles (voltage window of 1.5 V using H₂SO₄/PVA gel electrolyte) (Figure 8d). Using LiCl as an electrolyte, an asymmetric yarn supercapacitor consisting of a MXene/CNT yarn as the cathode and a MnO₂/CNT yarn as the anode demonstrated a large operation window of 2 V, and showed a high areal energy density of 100 μWh cm⁻² at a power density of 260 μW cm⁻².^[129]

The device structure has also been shown to affect the durability and performance of TSCs under mechanical deformation. Many works have demonstrated good bending

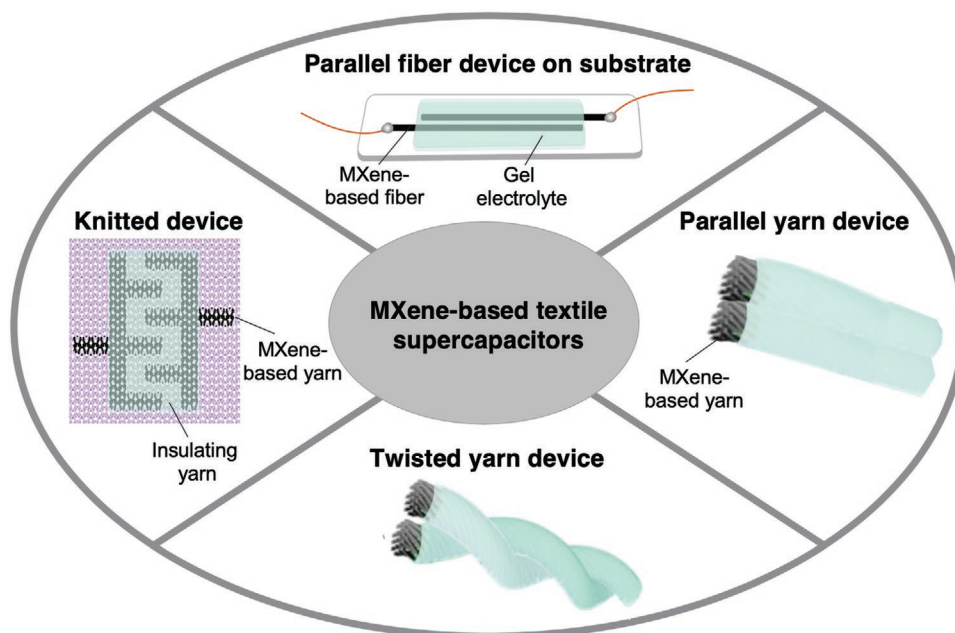


Figure 7. Symmetric textile supercapacitors developed using MXene-based fibers or yarns. Using two MXene-based fibers, devices are assembled on a planar substrate. MXene-based yarns are assembled into freestanding devices by placing the yarn electrodes in parallel with electrolyte in between or by twisting them together. Knitted devices are fabricated by knitting MXene-based yarns into two electrodes, with an insulating yarn acting as the separator.

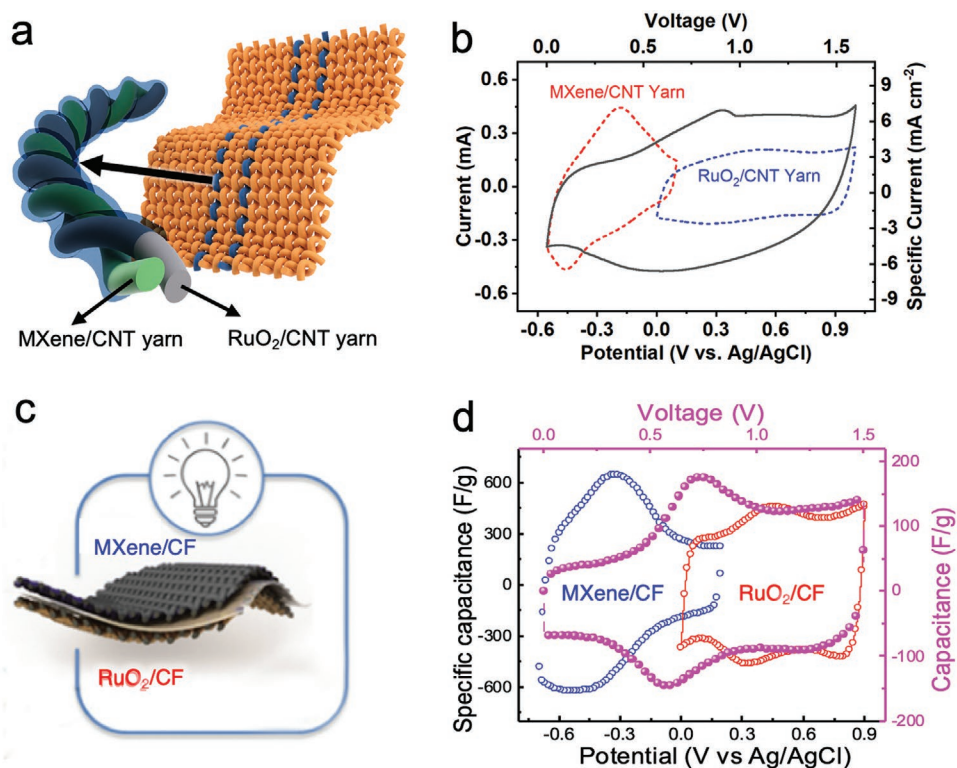


Figure 8. Asymmetric textile supercapacitors developed using MXene-based fibers and fabrics as cathodes. a) Schematic illustration of bisrolled MXene/CNT//RuO₂/CNT asymmetric TSCs woven into a textile. b) CV curves measured at a scan rate of 5 mV s⁻¹ showing the working potential range of the bisrolled MXene/CNT and bisrolled RuO₂/CNT yarn electrodes and a TSC device. Adapted with permission.^[100] Copyright 2018, WILEY-VCH. c) Schematic illustration of an RuO₂//Ti₃C₂T_x asymmetric pseudocapacitor. d) CVs of an RuO₂-coated CF (carbon fiber fabric) electrode, Ti₃C₂T_x-coated CF electrode, and an asymmetric device at a scan rate of 50 mV s⁻¹. Adapted with permission.^[98] Copyright 2018, WILEY-VCH.

performance of parallel MXene-based fiber supercapacitors and yarn supercapacitors mounted onto plastic substrates, but these architectures are not practical for integration into textiles.^[107,111,112] To produce freestanding fiber and yarn supercapacitors, the twisted structure is widely adopted. For example, freestanding bisrolled MXene/CNT yarns and bisrolled RuO₂/CNT yarns were twisted and coated with electrolyte and demonstrated a stable response when subjected to repeated bending cycles from 0°–180°. Furthermore, the capacitance retention was nearly 100%, and the yarn supercapacitor was sewn into cotton fabric.^[100] Comparing the durability of parallel, twisted, and face-to-face configurations, it was found that the face-to-face configuration resulted in yarn supercapacitors with the highest capacitance retention exceeding 95% under different deformation modes, i.e., horizontal bending, longitudinal bending, and twisting under various angles.^[38]

The effect of device length on the electrochemical performance of MXene-based fiber and yarn supercapacitors has also been studied. Most of the MXene-based fiber devices reported to date were 1–5 cm in length, including bisrolled MXene/CNT yarn-based devices, which were ≈5 cm long^[100,118] and MXene/rGO fiber-based devices, which were ≈1 cm long.^[53,111,112] Producing longer MXene-based fiber and yarn supercapacitors would open new avenues and applications for these devices, including the fabrication of stretchable supercapacitors,^[36] where fiber- and yarn-based devices are wrapped around elastic substrates, and integration into textiles using industrial textile manufacturing equipment. One challenge related to the performance of long fiber and yarn supercapacitors is that the resistance of the fiber/yarn electrodes scales linearly with length. A strategy to improve the electrical conductivity of fiber electrodes over long lengths is to use a commercial conductive yarn as a current collector, such as carbon fiber or silver-coated nylon yarn. For example, MXene-coated carbon fibers were assembled into symmetric supercapacitors up to 30 cm in length and the total capacitance increased from ≈0.4 to ≈2.1 F as the length increased from 3 to 30 cm, respectively.^[38] However, the length-specific capacitance of the device decreased from ≈131.7 mF cm⁻¹ (3 cm) to 71.4 mF cm⁻¹ (30 cm) when the electrode length increased. These results demonstrate that the total capacitance of MXene-based yarn supercapacitors is improved by increasing the length of the device, but the length-specific performance is reduced.

Another approach to mitigate the issue of length-specific capacitance decreasing as a function of yarn length is to knit MXene-coated yarns into fabric electrodes, providing multiple pathways for the flow of charges. Recently, MXene-coated cotton and nylon yarns were knitted into TSC geometries. A gel electrolyte was drop-cast onto the devices after knitting. Many supercapacitor designs were knitted, including vertically striped electrodes, horizontally striped electrodes, and interdigitated electrodes.^[96] It was found that the geometry (length and width of electrodes) and structure of the textile (stitch density and stitch type) affected the capacitance and rate capability of knitted supercapacitors. For example, increasing the density of stitches by changing the stitch pattern resulted in a 36% increase in areal capacitance at 2 mV s⁻¹ (from 520 to

707 mF cm⁻² in 1 M H₃PO₄) and almost a 50% increase at 50 mV s⁻¹ (211 vs 109 mF cm⁻²). Additionally, by changing the type and arrangement of stitches, the spacing between electrodes decreased from 2.8 mm to 600 μm. In doing so, the areal capacitance increased from 402 mF cm⁻² to 707 mF cm⁻² at 2 mV s⁻¹.^[96]

4.5. Textile Manufacturing Feasibility

While many coating and spinning techniques have been explored to introduce MXene into fibers, the next step in developing textile-based wearable supercapacitors is to incorporate these fibers into textiles. Many of the works discussed in this section integrated MXene-based fibers into textiles by hand stitching, knitting, or embroidering, including bisrolled MXene/CNT-based devices, which were hand-stitched into woven cotton fabric.^[100] Similarly, MXene/GO wet-spun fibers were co-knitted with nylon yarn using an 8-needle manually operated circular weft knitting machine.^[111] These works demonstrated the first step toward textile integration.

Recently, the first studies on knitting MXene-based fibers and yarns on an industrial knitting machine were reported.^[40,41,96] MXene/PU wet-spun fibers, MXene-coated cotton fibers, MXene-coated bamboo fibers, and MXene-coated nylon fibers were knitted into textile devices using a Shima Seiki 041N knitting machine. Using this equipment, MXene-based fibers can be fabricated into porous and dense textile structures depending on the selected knit stitches.^[40] Furthermore, complex textile structures and patterns can be designed, enabling the development of 3D knitted supercapacitors, discussed above.^[96]

5. Challenges and Outlook

Many forms and compositions of MXene-based fibers and yarns have been developed and studied over the last two years. However, great challenges and opportunities still exist in fabricating continuous fibers and yarns with excellent mechanical, electrical, and electrochemical properties. Beyond these properties, the long-term stability, durability, and environmental impact of MXene-based fibers, yarns, and textiles have yet to be fully studied. In this section, we highlight the challenges and opportunities during each step of the fiber/yarn fabrication process, from MXene synthesis, to fiber, yarn, and textile processing, property optimization, and device design. Addressing these challenges will not only enhance the performance of MXene-based TSCs, but the knowledge gained will be transferable to both the larger MXene community (in terms of synthesis, properties, and processing of MXenes) and the field of textile energy storage devices.

5.1. Large-Scale Production of Environmentally Stable MXenes

To assess the potential of scaling the production of MXene-based fibers to industrial quantities requires the synthesis of MXene on the kilogram scale. Delaminated Ti₃C₂T_x is currently

synthesized in 1–50 g batches;^[135] however, because MXene is synthesized via wet-chemical etching, there is great expectation to increase production by scaling the volume of etchants and the etching reactor to kilogram and ton quantities. Maintaining the quality of MXene (the exfoliation yield, flake size, elemental composition, etc.) when scaling up will be of great importance to address.^[135]

The production of large quantities of MXene brings about a number of safety and environmental concerns. The environmental impact of both synthesizing MXene and disposing of MXene-based materials is somewhat unknown. A process safety analysis for $Ti_3C_2T_x$ was recently reported, indicating that the major hazards during synthesis include dust ignition, runaway reactions, and toxic chemical exposure.^[136] Regarding chemical exposure, the synthesis of MXene requires the use of HF-containing etchant, which is a corrosive and toxic chemical. Another concern is handling the large quantity of waste produced during synthesis and assessing how these chemicals affect the environment.^[136] From these concerns, safer and more environmentally friendly synthesis methods would be desired. However, in the case of Ti-based MXenes (Ti_3C_2 , Ti_2C , or Ti_3CN), TiO_2 , and gaseous degradation products, such as CH_4 or $C O_2$, are fairly benign.

While the stability of both aqueous and organic MXene dispersions has been studied, a systematic study has yet to be conducted for dried MXene, such as freestanding films, prints, and fibers. Since these fiber electrodes will be used in textile applications, it is necessary that they reach or surpass the lifetime of conventional textiles. It is promising that MXene drawn on paper was monitored over a 6-month period with no noticeable fading or flaking of the MXene.^[137] Also, multiple washing cycles in water and a mild detergent only slightly decreased conductivity of MXene-coated cotton yarns.^[40] However, to truly understand the effects of water and oxygen on dried MXene, it will be necessary to monitor the properties (optical and electronic, for example) over a prolonged exposure time. It will also be important to study the effect of sunlight, laundering, abrasion, and friction on MXene TSC performance, although very few studies have touched upon this in the TSC community. These stability and durability studies would inform the long-term use of MXene-based fibers in textiles. With this information, preventive measures to reduce the effects of electrostatics and laundering, such as encapsulating TSCs with a protective layer, may be taken.

5.2. Expanding MXene-Based Fiber Processing Techniques

Currently, methods to spin MXene-based fibers have been largely limited to wet spinning and electrospinning. As previously mentioned, MXene composite fiber electrodes produced via conventional electrospinning methods may not be ideal for supercapacitor applications because MXene flakes get trapped inside of polymeric nanofibers, rendering them inaccessible to electrolyte ions. Therefore, more novel electrospinning methods or combined electrospinning and coating techniques are needed to integrate MXenes into nanofiber structures for this application. For example, spraying or electrospraying MXenes during nanofiber formation may result

in fiber mats or yarns with MXene flakes trapped between nanofibers, rather than inside of nanofibers. Many other spinning techniques, such as dry spinning,^[138] melt spinning,^[139] and thermal drawing,^[140] have been used to spin fibers from other 2D materials and conductive particles, but these methods have yet to be used to produce MXene-based fibers. These methods have many advantages over current methods. For example, dry spinning, as opposed to wet spinning, produces fibers without a coagulation bath, resulting in a faster spinning process. Melt spinning has an even higher production rate compared to wet spinning and dry spinning, manufacturing fibers at around $600\text{--}6000\text{ m min}^{-1}$.^[141] Melt spinning is also a solvent-free process, making it a more environmentally friendly and economical option. Thermal drawing is a method in which a preform is heated and drawn into a fiber. This method can be used to make complex fiber architectures, including fibers with embedded wires or other electronic components.^[140] MXene-based fibers have the potential to be processed via thermal drawing with assistance from polymers such as polymethyl methacrylate and high-density polyethylene. For example, preforms can be made for drawing by sandwiching MXene films between polymer sheets or mixing them together to form a homogenous composite. However, the processability of MXene at high temperatures has not been explored and therefore the structure of MXene will need to be carefully monitored during melt spinning and thermal drawing processes. If successful, these methods could lead to new avenues to produce long, continuous MXene-based fibers.

5.3. Enhancing Properties of MXene-Based Fibers

Although MXene-based fibers demonstrated excellent electrical and electrochemical properties, there is still much room for improvement. For instance, the limited voltage window of MXenes compared to other electrode materials has limited the energy density and other energy storage properties. For example, MXene has a smaller operation window (-0.7 to 0.2 V vs Ag/AgCl) than carbon-based materials (0 to 1.0 V vs Ag/AgCl) and PEDOT:PSS (-0.8 to 0.8 V vs Ag/AgCl) in $1\text{ M H}_2\text{SO}_4$. Another major challenge has been enhancing the tensile strength and strain-to-failure of fibers with high MXene loadings. Here, we suggest three promising approaches to enhance the electrochemical properties and/or mechanical of MXene-based fibers.

5.3.1. Surface Functionalization and Modification of MXenes

As discussed in Section 4, MXene-based fibers suffer from low mechanical strength in part because of poor interaction between flakes. It is expected that functionalizing the surface of MXene and/or using bridging agents may improve the mechanical strength of the resulting fibers. These modifications may result in improvements in electrochemical properties as well. Recent reports have demonstrated that changing the termination groups on flakes, by nitrogen doping, for example, enhanced the energy storage performance of MXene films,^[142] although this behavior requires

further verification. It would be interesting to see the effects of nitrogen doping and other surface modifications on MXene-based fibers.

5.3.2. Large MXene Flakes

The effects of MXene flake size on various properties, including mechanical, electrical, and electrochemical, have been discussed throughout this article. It has been demonstrated through numerous studies that films and fibers made from large flakes have higher electrical conductivity and mechanical strength than those made from small flakes. However, the size of these flakes is currently limited to $\approx 4 \mu\text{m}$ on average, which is significantly lower than the size of large graphene sheets ($50\text{--}100 \mu\text{m}$).^[10,61,120] To increase the size of flakes to tens of micrometers would require a MAX phase precursor with a large crystal size and efficient etching conditions to maintain the large flake size. These large flakes are expected to further enhance the electrical conductivity, environmental stability, and mechanical strength of fibers. These may also benefit new fiber processing methods, such as air-gap spinning or film scrolling, however, large flakes can also limit transport of ions and electrochemical performance of TSCs.

5.3.3. Electrolyte Selection

Ideal solid-state electrolytes for TSCs have high stability and flexibility, long lifetimes, wide voltage windows, and high ionic conductivity. They should also be nonflammable and environmentally friendly. Polymeric gel electrolytes, such as those based on PVA, have been used in the majority of TSC studies. However, their properties are far from the ideal requirements. For example, aqueous PVA-gel electrolytes have a limited operation window ($\approx 1 \text{ V}$) and are affected by heat and moisture. Using nonaqueous gel electrolytes would improve the energy density of MXene-based TSCs. Several attempts have been made to use organic electrolytes for MXene-based electrodes and while these systems have increased operation windows up to 1.8 V , the capacitance suffered due to the presence of solvent molecules between MXene layers, which influenced ionic transport and the total amount of charge able to be stored by the electrode.^[143] Several works on carbon-based TSCs demonstrated that redox electrolytes increased the operation window of TSCs.^[144,145] The charge-discharge mechanisms for MXenes in these electrolytes are currently unknown and further understanding of the capacitive behavior of MXenes in these electrolytes is needed to potentially improve the performance and stability of TSCs.

5.4. Other MXenes and Applications beyond Energy Storage

To date, over 30 different stoichiometric MXenes have been synthesized and density functional theory calculations predicted

more than 25 different ordered MXenes with 2 transition metals.^[24,49] About 100 stoichiometric MXenes and an infinite number of solid solutions are possible. However, the majority of works on MXenes have focused on $\text{Ti}_3\text{C}_2\text{T}_x$, attributing to its high electrical conductivity and volumetric capacitance. The capabilities of other MXenes are not fully known, but preliminary research indicates interesting properties beyond those of $\text{Ti}_3\text{C}_2\text{T}_x$ alone. For example, Nb_4C_3 has demonstrated higher strength compared to $\text{Ti}_3\text{C}_2\text{T}_x$ ^[146] and a wide range of optical properties (colors) can be produced using other MXene compositions.^[20]

In addition to exploring other MXenes for TSC applications, there are many other potential applications of MXene-based fibers. For instance, MXene films have demonstrated vast potential in gas sensing, EMI shielding,^[27] antennas,^[28] reinforcement for composites,^[70] and water purification,^[147] but these applications have been largely unexplored for MXene-based fibers. Recent works have demonstrated the use of MXene-based fibers for wearable heaters,^[39,148] fiber and textile strain sensors,^[41,148] EMI shielding, and textile pressure sensors^[40,95] (Figure 9).

5.5. Challenges of TSC

Many review articles have discussed challenges related to the production and use of TSCs, including durability, washing ability, scalability, and integration into textiles.^[44,149,150] However, few works have explored the aforementioned metrics on TSCs (MXene-based or otherwise). This is partly due to a lack of systematic methods to evaluate these properties. Taking durability as an example, the current standard in TSC literature is to test their electrochemical performance before and after bending at 45° , 90° , 180° , etc. In this process, a few important parameters are often ignored, such as the thickness of textile or fabric, bending radius, and bending force. Moreover, simple bending tests cannot represent the deformations that fibers and yarns experience during wear and do not account for abrasion or friction. Thus, the field needs to establish comprehensive test methods that more accurately represent the conditions that fibers and yarns experience in everyday use.

As for integration into textiles, there are two main challenges associated with the production of knitted and woven energy storage devices: i) scaling up the fiber electrodes from centimeters to meters; ii) Improving the mechanical properties for fibers to withstand the mechanical forces they will encounter during the textile fabrication process. Once these requirements are met, the advantages of industrial textile production are twofold. First, compared to manual techniques, industrial techniques are fast, scalable, more precise, and reproducible. Second, complex textile patterns can be designed, simulated, and prototyped using industrial techniques to, for example, reduce the resistance of yarns by increasing the number of contact points, increase the density of the textile to improve capacitance or shielding efficiency, or reduce spacing between electrodes (in the case of knit supercapacitors) to minimize the ion diffusion pathway.

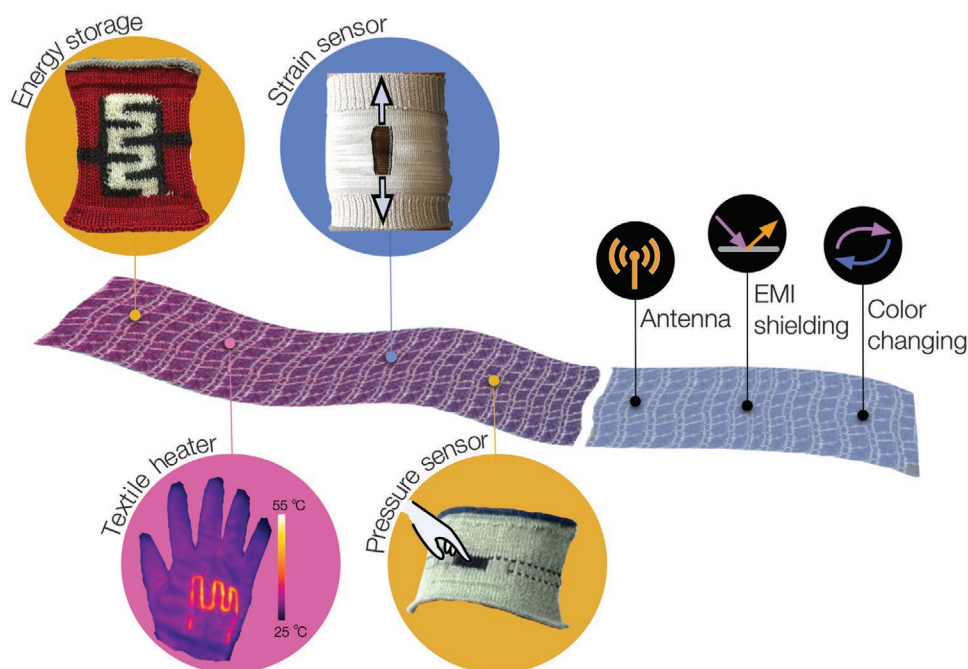


Figure 9. MXene-based fibers and yarns knitted into textile devices. Schematic illustration showing textile devices made using MXene-based fibers and yarns and promising applications of these fibers and yarns in textiles. A knitted energy storage device using MXene-coated cotton yarns as electrodes. Adapted with permission.^[96] Copyright 2020, Elsevier Ltd. A textile heater made by sewing MXene-coated polyester yarns into a woven cotton glove. Adapted with permission.^[39] Copyright 2019, American Chemical Society. A knitted pressure sensor button (active area: 16 mm × 5 mm). Adapted with permission.^[40] Copyright 2019, WILEY-VCH. An elbow sleeve knitted by using four ends of MXene/PU composite fiber. Adapted with permission.^[41] Copyright 2020, WILEY-VCH.

Acknowledgements

A.L. and J.Z. contributed equally to this work. J.M.R. acknowledges financial support from the Australian Research Council (Grant Nos. FT130100380, IH140100018, and DP170102859). A.L. was supported by the National Science Foundation Graduate Research Fellowship under Grant No. DGE-1646737. Any opinion, findings, and conclusion or recommendations expressed in this material were those of the authors and did not necessarily reflect the views of the National Science Foundation.

Conflict of Interest

The authors declare no conflict of interest.

Keywords

energy storage devices, fibers, MXene, textiles, yarns, wearable devices

Received: January 25, 2020

Revised: March 1, 2020

Published online:

[1] A. Viswanathan, *World Pat. Inf.* **2010**, 32, 300.

[2] H. Mera, T. Takata, in *Ullmann's Encyclopedia of Industrial Chemistry*, Wiley-VCH Verlag GmbH & Co., Weinheim **2000**.

[3] E. Fitzer, *Carbon* **1989**, 27, 621.

- [4] B. S. Shim, W. Chen, C. Doty, C. Xu, N. A. Kotov, *Nano Lett.* **2008**, 8, 4151.
- [5] D. Yu, Q. Qian, L. Wei, W. Jiang, K. Goh, J. Wei, J. Zhang, Y. Chen, *Chem. Soc. Rev.* **2015**, 44, 647.
- [6] S. H. Aboutalebi, R. Jalili, D. Esrafilzadeh, M. Salari, Z. Gholamvand, S. Aminorroaya Yamini, K. Konstantinov, R. L. Shepherd, J. Chen, S. E. Moulton, P. C. Innis, A. I. Minett, J. M. Razal, G. G. Wallace, *ACS Nano* **2014**, 8, 2456.
- [7] Y. Gogotsi, *Nature* **2014**, 509, 568.
- [8] K. Jost, D. P. Durkin, L. M. Haverhals, E. K. Brown, M. Langenstein, H. C. De Long, P. C. Trulove, Y. Gogotsi, G. Dion, *Adv. Energy Mater.* **2015**, 5, 1401286.
- [9] Z. Lu, R. Raad, F. Safaei, J. Xi, Z. Liu, J. Foroughi, *Front. Mater.* **2019**, 6, 138.
- [10] Z. Xu, H. Sun, X. Zhao, C. Gao, *Adv. Mater.* **2013**, 25, 188.
- [11] S. Chen, W. Ma, Y. Cheng, Z. Weng, B. Sun, L. Wang, W. Chen, F. Li, M. Zhu, H.-M. Cheng, *Nano Energy* **2015**, 15, 642.
- [12] C.-M. Yang, B.-H. Kim, *J. Alloys Compd.* **2018**, 749, 441.
- [13] N. Yu, H. Yin, W. Zhang, Y. Liu, Z. Tang, M.-Q. Zhu, *Adv. Energy Mater.* **2016**, 6, 1501458.
- [14] X. Li, D. Liu, X. Yin, C. Zhang, P. Cheng, H. Guo, W. Song, J. Wang, *J. Power Sources* **2019**, 440, 227143.
- [15] J. Xu, Q. Wang, X. Wang, Q. Xiang, B. Liang, D. Chen, G. Shen, *ACS Nano* **2013**, 7, 5453.
- [16] S. Zhai, C. Wang, H. E. Karahan, Y. Wang, X. Chen, X. Sui, Q. Huang, X. Liao, X. Wang, Y. Chen, *Small* **2018**, 14, 1800582.
- [17] K. Wang, Q. Meng, Y. Zhang, Z. Wei, M. Miao, *Adv. Mater.* **2013**, 25, 1494.
- [18] J. Zhang, S. Seyedin, S. Qin, P. A. Lynch, Z. Wang, W. Yang, X. Wang, J. M. Razal, *J. Mater. Chem. A* **2019**, 7, 6401.
- [19] V. Augustyn, P. Simon, B. Dunn, *Energy Environ. Sci.* **2014**, 7, 1597.

- [20] B. Anasori, Y. Gogotsi, *2D Metal Carbides and Nitrides (MXenes)*, Springer International Publishing, Cham **2019**.
- [21] M. Naguib, V. N. Mochalin, M. W. Barsoum, Y. Gogotsi, *Adv. Mater.* **2014**, *26*, 992.
- [22] G. Deysher, C. E. Shuck, K. Hantanasirisakul, N. C. Frey, A. C. Foucher, K. Maleski, A. Sarycheva, V. B. Shenoy, E. A. Stach, B. Anasori, Y. Gogotsi, *ACS Nano* **2020**, *14*, 204.
- [23] M. Naguib, M. Kurtoglu, V. Presser, J. Lu, J. Niu, M. Heon, L. Hultman, Y. Gogotsi, M. W. Barsoum, *Adv. Mater.* **2011**, *23*, 4248.
- [24] B. Anasori, Y. Xie, M. Beidaghi, J. Lu, B. C. Hosler, L. Hultman, P. R. C. Kent, Y. Gogotsi, M. W. Barsoum, *ACS Nano* **2015**, *9*, 9507.
- [25] M. R. Lukatskaya, S. Kota, Z. Lin, M.-Q. Zhao, N. Shpigel, M. D. Levi, J. Halim, P.-L. Taberna, M. W. Barsoum, P. Simon, Y. Gogotsi, *Nat. Energy* **2017**, *2*, 17105.
- [26] P. Srimuk, J. Halim, J. Lee, Q. Tao, J. Rosen, V. Presser, *ACS Sustainable Chem. Eng.* **2018**, *6*, 3739.
- [27] F. Shahzad, M. Alhabeab, C. B. Hatter, B. Anasori, S. Man Hong, C. M. Koo, Y. Gogotsi, *Science* **2016**, *353*, 1137.
- [28] A. Sarycheva, A. Polemi, Y. Liu, K. Dandekar, B. Anasori, Y. Gogotsi, *Sci. Adv.* **2018**, *4*, eaau0920.
- [29] J. Zhang, N. Kong, S. Uzun, A. Levitt, S. Seyedin, P. A. Lynch, S. Qin, M. Han, W. Yang, J. Liu, X. Wang, Y. Gogotsi, J. M. Razal, *Adv. Mater.* **2020**, 2001093.
- [30] L. Chen, Y. Liu, Y. Zhao, N. Chen, L. Qu, *Nanotechnology* **2016**, *27*, 032001.
- [31] K. Hantanasirisakul, M.-Q. Zhao, P. Urbankowski, J. Halim, B. Anasori, S. Kota, C. E. Ren, M. W. Barsoum, Y. Gogotsi, *Adv. Electron. Mater.* **2016**, *2*, 1600050.
- [32] A. D. Dillon, M. J. Ghidui, A. L. Krick, J. Griggs, S. J. May, Y. Gogotsi, M. W. Barsoum, A. T. Fafarman, *Adv. Funct. Mater.* **2016**, *26*, 4162.
- [33] C. Zhang, M. P. Kremer, A. Seral-Ascaso, S.-H. Park, N. McEvoy, B. Anasori, Y. Gogotsi, V. Nicolosi, *Adv. Funct. Mater.* **2018**, *28*, 1705506.
- [34] B. Akuzum, K. Maleski, B. Anasori, P. Lelyukh, N. J. Alvarez, E. C. Kumbur, Y. Gogotsi, *ACS Nano* **2018**, *12*, 2685.
- [35] K. Maleski, V. N. Mochalin, Y. Gogotsi, *Chem. Mater.* **2017**, *29*, 1632.
- [36] S. Seyedin, J. Zhang, K. A. S. Usman, S. Qin, A. M. Glushenkov, E. R. S. Yanza, R. T. Jones, J. M. Razal, *Global Challenges* **2019**, *3*, 1900037.
- [37] M. Hu, Z. Li, G. Li, T. Hu, C. Zhang, X. Wang, *Adv. Mater. Technol.* **2017**, *2*, 1700143.
- [38] J. Zhang, S. Seyedin, Z. Gu, W. Yang, X. Wang, J. M. Razal, *Nanoscale* **2017**, *9*, 18604.
- [39] T. H. Park, S. Yu, M. Koo, H. Kim, E. H. Kim, J.-E. Park, B. Ok, B. Kim, S. H. Noh, C. Park, E. Kim, C. M. Koo, C. Park, *ACS Nano* **2019**, *13*, 6835.
- [40] S. Uzun, S. Seyedin, A. L. Stoltzfus, A. S. Levitt, M. Alhabeab, M. Anayee, C. J. Strobel, J. M. Razal, G. Dion, Y. Gogotsi, *Adv. Funct. Mater.* **2019**, *29*, 1905015.
- [41] S. Seyedin, S. Uzun, A. Levitt, B. Anasori, G. Dion, Y. Gogotsi, J. M. Razal, *Adv. Funct. Mater.* **2020**, *30*, 1910504.
- [42] S. Zhai, H. E. Karahan, C. Wang, Z. Pei, L. Wei, Y. Chen, *Adv. Mater.* **2020**, *32*, 1902387.
- [43] M. Liao, L. Ye, Y. Zhang, T. Chen, H. Peng, *Adv. Electron. Mater.* **2019**, *5*, 1800456.
- [44] D. Chen, K. Jiang, T. Huang, G. Shen, *Adv. Mater.* **2020**, *32*, 1901806.
- [45] P. Kumar, U. N. Maiti, K. E. Lee, S. O. Kim, *Carbon* **2014**, *80*, 453.
- [46] W. Yang, J. Yang, J. J. Byun, F. P. Moissinac, J. Xu, S. J. Haigh, M. Domingos, M. A. Bissett, R. A. W. Dryfe, S. Barg, *Adv. Mater.* **2019**, *31*, 1902725.
- [47] C. J. Zhang, L. McKeon, M. P. Kremer, S. H. Park, O. Ronan, A. Seral-Ascaso, S. Barwich, C. O. Coileain, N. McEvoy, H. C. Nerl, B. Anasori, J. N. Coleman, Y. Gogotsi, V. Nicolosi, *Nat. Commun.* **2019**, *10*, 1795.
- [48] M. Alhabeab, K. Maleski, B. Anasori, P. Lelyukh, L. Clark, S. Sin, Y. Gogotsi, *Chem. Mater.* **2017**, *29*, 7633.
- [49] B. Anasori, M. R. Lukatskaya, Y. Gogotsi, *Nat. Rev. Mater.* **2017**, *2*, 16098.
- [50] O. Mashtalir, M. Naguib, V. N. Mochalin, Y. Dall'Agnese, M. Heon, M. W. Barsoum, Y. Gogotsi, *Nat. Commun.* **2013**, *4*, 1716.
- [51] M. Naguib, R. R. Unocic, B. L. Armstrong, J. Nanda, *Dalton Trans.* **2015**, *44*, 9353.
- [52] A. S. Levitt, M. Alhabeab, C. B. Hatter, A. Sarycheva, G. Dion, Y. Gogotsi, *J. Mater. Chem. A* **2019**, *7*, 269.
- [53] M. Lu, Z. Zhang, L. Kang, X. He, Q. Li, J. Sun, R. Jiang, H. Xu, F. Shi, Z. Lei, Z.-H. Liu, *J. Mater. Chem. A* **2019**, *7*, 12582.
- [54] O. Mashtalir, M. Naguib, B. Dyatkin, Y. Gogotsi, M. W. Barsoum, *Mater. Chem. Phys.* **2013**, *139*, 147.
- [55] C. E. Shuck, M. Han, K. Maleski, K. Hantanasirisakul, S. J. Kim, J. Choi, W. E. B. Reil, Y. Gogotsi, *ACS Appl. Nano Mater.* **2019**, *2*, 3368.
- [56] J. Zhang, S. Uzun, S. Seyedin, P. A. Lynch, B. Akuzum, Z. Wang, S. Qin, M. Alhabeab, C. E. Shuck, W. Lei, E. C. Kumbur, W. Yang, X. Wang, G. Dion, J. M. Razal, Y. Gogotsi, *ACS Cent. Sci.* **2020**, *6*, 254.
- [57] Y. Xia, T. S. Mathis, M.-Q. Zhao, B. Anasori, A. Dang, Z. Zhou, H. Cho, Y. Gogotsi, S. Yang, *Nature* **2018**, *557*, 409.
- [58] S. H. Aboutalebi, M. M. Gudarzi, Q. B. Zheng, J.-K. Kim, *Adv. Funct. Mater.* **2011**, *21*, 2978.
- [59] R. Jalili, S. H. Aboutalebi, D. Esrafilzadeh, R. L. Shepherd, J. Chen, S. Aminorroaya-Yamini, K. Konstantinov, A. I. Minett, J. M. Razal, G. G. Wallace, *Adv. Funct. Mater.* **2013**, *23*, 5345.
- [60] R. Jalili, S. H. Aboutalebi, D. Esrafilzadeh, K. Konstantinov, J. M. Razal, S. E. Moulton, G. G. Wallace, *Mater. Horiz.* **2014**, *1*, 87.
- [61] J. Zhang, S. Seyedin, Z. Gu, N. Salim, X. Wang, J. M. Razal, *Part. Part. Syst. Character.* **2017**, *34*, 1600396.
- [62] Q. Tian, Z. Xu, Y. Liu, B. Fang, L. Peng, J. Xi, Z. Li, C. Gao, *Nanoscale* **2017**, *9*, 12335.
- [63] S. Seyedin, M. S. Romano, A. I. Minett, J. M. Razal, *Sci. Rep.* **2015**, *5*, 14946.
- [64] K. Maleski, C. E. Ren, M.-Q. Zhao, B. Anasori, Y. Gogotsi, *ACS Appl. Mater. Interfaces* **2018**, *10*, 24491.
- [65] M. Ghidui, M. R. Lukatskaya, M.-Q. Zhao, Y. Gogotsi, M. W. Barsoum, *Nature* **2014**, *516*, 78.
- [66] A. Lipatov, M. Alhabeab, M. R. Lukatskaya, A. Boson, Y. Gogotsi, A. Sinitiskii, *Adv. Electron. Mater.* **2016**, *2*, 1600255.
- [67] A. Lipatov, H. Lu, M. Alhabeab, B. Anasori, A. Gruverman, Y. Gogotsi, A. Sinitiskii, *Sci. Adv.* **2018**, *4*, eaat0491.
- [68] M. Hu, T. Hu, R. Cheng, J. Yang, C. Cui, C. Zhang, X. Wang, *J. Energy Chem.* **2018**, *27*, 161.
- [69] M. Naguib, J. Halim, J. Lu, K. M. Cook, L. Hultman, Y. Gogotsi, M. W. Barsoum, *J. Am. Chem. Soc.* **2013**, *135*, 15966.
- [70] Z. Ling, C. E. Ren, M.-Q. Zhao, J. Yang, J. M. Giammarco, J. Qiu, M. W. Barsoum, Y. Gogotsi, *Proc. Natl. Acad. Sci. USA* **2014**, *111*, 16676.
- [71] C. E. Ren, K. B. Hatzell, M. Alhabeab, Z. Ling, K. A. Mahmoud, Y. Gogotsi, *J. Phys. Chem. Lett.* **2015**, *6*, 4026.
- [72] L. Lorencova, T. Bertok, E. Dosekova, A. Holazova, D. Paprckova, A. Vikartovska, V. Sasinkova, J. Filip, P. Kasak, M. Jerigova, D. Velic, K. A. Mahmoud, J. Tkac, *Electrochim. Acta* **2017**, *235*, 471.
- [73] M. A. Hope, A. C. Forse, K. J. Griffith, M. R. Lukatskaya, M. Ghidui, Y. Gogotsi, C. P. Grey, *Phys. Chem. Chem. Phys.* **2016**, *18*, 5099.
- [74] C. J. Zhang, S. Pinilla, N. McEvoy, C. P. Cullen, B. Anasori, E. Long, S.-H. Park, A. Seral-Ascaso, A. Shmeliyov, D. Krishnan, C. Morant, X. Liu, G. S. Duesberg, Y. Gogotsi, V. Nicolosi, *Chem. Mater.* **2017**, *29*, 4848.
- [75] V. Natu, M. Sokol, L. Verger, M. W. Barsoum, *J. Phys. Chem. C* **2018**, *122*, 27745.

- [76] Y. Deng, T. Shang, Z. Wu, Y. Tao, C. Luo, J. Liang, D. Han, R. Lyu, C. Qi, W. Lv, F. Kang, Q.-H. Yang, *Adv. Mater.* **2019**, *31*, 1902432.
- [77] A. M. Navarro-Suárez, C. Maleski, T. Makaryan, J. Yan, B. Anasori, Y. Gogotsi, *Batteries Supercaps* **2018**, *1*, 33.
- [78] S. Naficy, R. Jalili, S. H. Aboutaleb, R. A. Gorkin III, K. Konstantinov, P. C. Innis, G. M. Spinks, P. Poulin, G. G. Wallace, *Mater. Horiz.* **2014**, *1*, 326.
- [79] N. Behabtu, C. C. Young, D. E. Tsentelovich, O. Kleinerman, X. Wang, A. W. K. Ma, E. A. Bengio, R. F. ter Waarbeek, J. J. de Jong, R. E. Hoogerwerf, S. B. Fairchild, J. B. Ferguson, B. Maruyama, J. Kono, Y. Talmon, Y. Cohen, M. J. Otto, M. Pasquali, *Science* **2013**, *339*, 182.
- [80] L. Onsager, *Ann. N. Y. Acad. Sci.* **1949**, *51*, 627.
- [81] V. A. Davis, A. N. G. Parra-Vasquez, M. J. Green, P. K. Rai, N. Behabtu, V. Prieto, R. D. Booker, J. Schmidt, E. Kesselman, W. Zhou, H. Fan, W. W. Adams, R. H. Hauge, J. E. Fischer, Y. Cohen, Y. Talmon, R. E. Smalley, M. Pasquali, *Nat. Nanotechnol.* **2009**, *4*, 830.
- [82] Z. Xu, C. Gao, *Acc. Chem. Res.* **2014**, *47*, 1267.
- [83] J. P. Canejo, J. P. Borges, M. H. Godinho, P. Brogueira, P. I. C. Teixeira, E. M. Terentjev, *Adv. Mater.* **2008**, *20*, 4821.
- [84] S. Chen, G. Schueneman, R. B. Pipes, J. Youngblood, R. J. Moon, *Biomacromolecules* **2014**, *15*, 3827.
- [85] S. Iwamoto, A. Isogai, T. Iwata, *Biomacromolecules* **2011**, *12*, 831.
- [86] K. Jost, D. Stenger, C. R. Perez, J. K. McDonough, K. Lian, Y. Gogotsi, G. Dion, *Energy Environ. Sci.* **2013**, *6*, 2698.
- [87] L. Liu, Y. Yu, C. Yan, K. Li, Z. Zheng, *Nat. Commun.* **2015**, *6*, 7260.
- [88] N. Karim, S. Afroj, S. Tan, P. He, A. Fernando, C. Carr, K. S. Novoselov, *ACS Nano* **2017**, *11*, 12266.
- [89] Y. Shao, M. F. El-Kady, L. J. Wang, Q. Zhang, Y. Li, H. Wang, M. F. Mousavi, R. B. Kaner, *Chem. Soc. Rev.* **2015**, *44*, 3639.
- [90] Y. Huang, H. Hu, Y. Huang, M. Zhu, W. Meng, C. Liu, Z. Pei, C. Hao, Z. Wang, C. Zhi, *ACS Nano* **2015**, *9*, 4766.
- [91] K. Guo, Y. Ma, H. Li, T. Zhai, *Small* **2016**, *12*, 1024.
- [92] Z. Xu, C. Gao, *Nat. Commun.* **2011**, *2*, 571.
- [93] H. Park, K. H. Lee, Y. B. Kim, S. B. Ambade, S. H. Noh, W. Eom, J. Y. Hwang, W. J. Lee, J. Huang, T. H. Han, *Sci. Adv.* **2018**, *4*, eaau2104.
- [94] R. Cruz-Silva, A. Morelos-Gomez, H.-i. Kim, H.-k. Jang, F. Tristan, S. Vega-Díaz, L. P. Rajukumar, A. L. Elías, N. Perea-Lopez, J. Suhr, M. Endo, M. Terrones, *ACS Nano* **2014**, *8*, 5959.
- [95] T. Li, L. Chen, X. Yang, X. Chen, Z. Zhang, T. Zhao, X. Li, J. Zhang, *J. Mater. Chem. C* **2019**, *7*, 1022.
- [96] A. Levitt, D. Hegh, P. Phillips, S. Uzun, M. Anayee, J. M. Razal, Y. Gogotsi, G. Dion, *Mater. Today* **2020**, *34*, 17.
- [97] J. A. Lee, M. K. Shin, S. H. Kim, H. U. Cho, G. M. Spinks, G. G. Wallace, M. D. Lima, X. Lepró, M. E. Kozlov, R. H. Baughman, S. J. Kim, *Nat. Commun.* **2013**, *4*, 1970.
- [98] Q. Jiang, N. Kurra, M. Alhabeb, Y. Gogotsi, H. N. Alshareef, *Adv. Energy Mater.* **2018**, *8*, 1703043.
- [99] J. Zhang, S. Seyedin, S. Qin, Z. Wang, S. Moradi, F. Yang, P. A. Lynch, W. Yang, J. Liu, X. Wang, J. M. Razal, *Small* **2019**, *15*, 1804732.
- [100] Z. Wang, S. Qin, S. Seyedin, J. Zhang, J. Wang, A. Levitt, N. Li, C. Haines, R. Ovalle-Robles, W. Lei, Y. Gogotsi, R. H. Baughman, J. M. Razal, *Small* **2018**, *14*, 1802225.
- [101] Z. Zhou, W. Panatdasirisuk, T. S. Mathis, B. Anasori, C. Lu, X. Zhang, Z. Liao, Y. Gogotsi, S. Yang, *Nanoscale* **2018**, *10*, 6005.
- [102] A. Singh, V. Kalra, *J. Mater. Chem. A* **2019**, *7*, 11613.
- [103] C. J. Zhang, S. H. Park, A. Seral-Ascaso, S. Barwich, N. McEvoy, C. S. Boland, J. N. Coleman, Y. Gogotsi, V. Nicolosi, *Nat. Commun.* **2019**, *10*, 849.
- [104] F. Xiong, Z. Cai, L. Qu, P. Zhang, Z. Yuan, O. K. Asare, W. Xu, C. Lin, L. Mai, *ACS Appl. Mater. Interfaces* **2015**, *7*, 12625.
- [105] E. A. Mayerberger, R. M. Street, R. M. McDaniel, M. W. Barsoum, C. L. Schauer, *RSC Adv.* **2018**, *8*, 35386.
- [106] E. A. Mayerberger, O. Urbanek, R. M. McDaniel, R. M. Street, M. W. Barsoum, C. L. Schauer, *J. Appl. Polym. Sci.* **2017**, *134*, 45295.
- [107] W. Shao, M. Tebyetekerwa, I. Marriam, W. Li, Y. Wu, S. Peng, S. Ramakrishna, S. Yang, M. Zhu, *J. Power Sources* **2018**, *396*, 683.
- [108] J. Mu, M. Jung de Andrade, S. Fang, X. Wang, E. Gao, N. Li, S. H. Kim, H. Wang, C. Hou, Q. Zhang, M. Zhu, D. Qian, H. Lu, D. Kongahage, S. Talebian, J. Foroughi, G. Spinks, H. Kim, T. H. Ware, H. J. Sim, D. Y. Lee, Y. Jang, S. J. Kim, R. H. Baughman, *Science* **2019**, *365*, 150.
- [109] H. Okuzaki, M. Ishihara, *Macromol. Rapid Commun.* **2003**, *24*, 261.
- [110] R. Jalili, J. M. Razal, P. C. Innis, G. G. Wallace, *Adv. Funct. Mater.* **2011**, *21*, 3363.
- [111] S. Seyedin, E. R. S. Yanza, J. M. Razal, *J. Mater. Chem. A* **2017**, *5*, 24076.
- [112] Q. Yang, Z. Xu, B. Fang, T. Huang, S. Cai, H. Chen, Y. Liu, K. Gopalsamy, W. Gao, C. Gao, *J. Mater. Chem. A* **2017**, *5*, 22113.
- [113] M. D. Lima, S. Fang, X. Lepró, C. Lewis, R. Ovalle-Robles, J. Carretero-González, E. Castillo-Martínez, M. E. Kozlov, J. Oh, N. Rawat, C. S. Haines, M. H. Haque, V. Aare, S. Stoughton, A. A. Zakhidov, R. H. Baughman, *Science* **2011**, *331*, 51.
- [114] C. Choi, K. M. Kim, K. J. Kim, X. Lepró, G. M. Spinks, R. H. Baughman, S. J. Kim, *Nat. Commun.* **2016**, *7*, 13811.
- [115] C. Choi, J. A. Lee, A. Y. Choi, Y. T. Kim, X. Lepró, M. D. Lima, R. H. Baughman, S. J. Kim, *Adv. Mater.* **2014**, *26*, 2059.
- [116] A. Helland, P. Wick, A. Koehler, K. Schmid, C. Som, *Environ. Health Perspect.* **2007**, *115*, 1125.
- [117] A. D. Maynard, P. A. Baron, M. Foley, A. A. Shvedova, E. R. Kisin, V. Castranova, *J. Toxicol. Environ. Health, Part A* **2004**, *67*, 87.
- [118] C. Yu, Y. Gong, R. Chen, M. Zhang, J. Zhou, J. An, F. Lv, S. Guo, G. Sun, *Small* **2018**, *14*, 1801203.
- [119] J. Zhang, S. Seyedin, S. Qin, Z. Wang, S. Moradi, F. Yang, P. A. Lynch, W. Yang, J. Liu, X. Wang, J. M. Razal, *Small* **2019**, *15*, 1970041.
- [120] C. Xiang, C. C. Young, X. Wang, Z. Yan, C.-C. Hwang, G. Ceriotti, J. Lin, J. Kono, M. Pasquali, J. M. Tour, *Adv. Mater.* **2013**, *25*, 4592.
- [121] M. Z. Seyedin, J. M. Razal, P. C. Innis, R. Jalili, G. G. Wallace, *Adv. Funct. Mater.* **2015**, *25*, 94.
- [122] F. Meng, W. Lu, Q. Li, J.-H. Byun, Y. Oh, T.-W. Chou, *Adv. Mater.* **2015**, *27*, 5113.
- [123] C. Zhang, B. Anasori, A. Seral-Ascaso, S.-H. Park, N. McEvoy, A. Shmeliov, G. S. Duesberg, J. N. Coleman, Y. Gogotsi, V. Nicolosi, *Adv. Mater.* **2017**, *29*, 1702678.
- [124] Z. Xu, Z. Liu, H. Sun, C. Gao, *Adv. Mater.* **2013**, *25*, 3249.
- [125] Y. Li, H. Zhu, F. Shen, J. Wan, X. Han, J. Dai, H. Dai, L. Hu, *Adv. Funct. Mater.* **2014**, *24*, 7366.
- [126] X. Wang, T. S. Mathis, K. Li, Z. Lin, L. Vlcek, T. Torita, N. C. Osti, C. Hatter, P. Urbankowski, A. Sarycheva, M. Tyagi, E. Mamontov, P. Simon, Y. Gogotsi, *Nat. Energy* **2019**, *4*, 241.
- [127] Y.-Y. Peng, B. Akuzum, N. Kurra, M.-Q. Zhao, M. Alhabeb, B. Anasori, E. C. Kumbur, H. N. Alshareef, M.-D. Ger, Y. Gogotsi, *Energy Environ. Sci.* **2016**, *9*, 2847.
- [128] S. Zhai, W. Jiang, L. Wei, H. E. Karahan, Y. Yuan, A. K. Ng, Y. Chen, *Mater. Horiz.* **2015**, *2*, 598.
- [129] J. W. Park, D. Y. Lee, H. Kim, J. S. Hyeon, M. J. de Andrade, R. H. Baughman, S. J. Kim, *MRS Commun.* **2019**, *9*, 114.
- [130] A. Sugahara, Y. Ando, S. Kajiyama, K. Yazawa, K. Gotoh, M. Otani, M. Okubo, A. Yamada, *Nat. Commun.* **2019**, *10*, 850.
- [131] C. Couly, M. Alhabeb, K. L. Van Aken, N. Kurra, L. Gomes, A. M. Navarro-Suárez, B. Anasori, H. N. Alshareef, Y. Gogotsi, *Adv. Electron. Mater.* **2018**, *4*, 1700339.
- [132] X. Yang, C. Cheng, Y. Wang, L. Qiu, D. Li, *Science* **2013**, *341*, 534.
- [133] M. D. Stoller, S. Park, Y. Zhu, J. An, R. S. Ruoff, *Nano Lett.* **2008**, *8*, 3498.
- [134] C.-C. Hu, K.-H. Chang, M.-C. Lin, Y.-T. Wu, *Nano Lett.* **2006**, *6*, 2690.

- [135] C. E. Shuck, A. Sarycheva, M. Anayee, A. Levitt, Y. Zhu, S. Uzun, V. Balitskiy, V. Zahorodna, O. Gogotsi, Y. Gogotsi, *Adv. Eng. Mater.* **2020**, *22*, 1901241.
- [136] P. Lakhe, E. M. Prehn, T. Habib, J. L. Lutkenhaus, M. Radovic, M. S. Mannan, M. J. Green, *Ind. Eng. Chem. Res.* **2019**, *58*, 1570.
- [137] E. Quain, T. S. Mathis, N. Kurra, K. Maleski, K. L. Van Aken, M. Alhabeab, H. N. Alshareef, Y. Gogotsi, *Adv. Mater. Technol.* **2019**, *4*, 1800256.
- [138] L. Feng, Y. Chang, J. Zhong, D.-C. Jia, *Sci. Rep.* **2018**, *8*, 10803.
- [139] B. Weise, L. Völkel, G. Köppe, S. Schriever, J. Mroszczok, J. Köhler, P. Scheffler, M. Wegener, G. Seide, *Mater. Today: Proc.* **2017**, *4*, S135.
- [140] M. Bayindir, A. F. Abouraddy, O. Shapira, J. Viens, D. Saygin-Hinczewski, F. Sorin, J. Arnold, J. D. Joannopoulos, Y. Fink, *IEEE J. Sel. Top. Quantum Electron.* **2006**, *12*, 1202.
- [141] V. B. Gupta, *Manufactured Fibre Technology*, Springer International Publishing, Cham **1997**.
- [142] C. Yang, Y. Tang, Y. Tian, Y. Luo, M. Faraz Ud Din, X. Yin, W. Que, *Adv. Energy Mater.* **2018**, *8*, 1802087.
- [143] Y. Dall'Agnese, P. Rozier, P.-L. Taberna, Y. Gogotsi, P. Simon, *J. Power Sources* **2016**, *306*, 510.
- [144] S. Roldán, C. Blanco, M. Granda, R. Menéndez, R. Santamaría, *Angew. Chem., Int. Ed.* **2011**, *50*, 1699.
- [145] S. T. Senthilkumar, R. K. Selvan, J. S. Melo, *J. Mater. Chem. A* **2013**, *1*, 12386.
- [146] A. Lipatov, M. Alhabeab, H. Lu, S. Zhao, M. Loes, N. S. Vorobeva, Y. Dall'Agnese, Y. Gao, A. Gruverman, Y. Gogotsi, A. Sinitskii, *Adv. Electron. Mater.* **2020**, 1901382.
- [147] L. Ding, Y. Wei, Y. Wang, H. Chen, J. Caro, H. Wang, *Angew. Chem., Int. Ed.* **2017**, *56*, 1825.
- [148] W. T. Cao, C. Ma, D. S. Mao, J. Zhang, M. G. Ma, F. Chen, *Adv. Funct. Mater.* **2019**, *29*, 1905898.
- [149] M. Tebyetekerwa, I. Marriam, Z. Xu, S. Yang, H. Zhang, F. Zabih, R. Jose, S. Peng, M. Zhu, S. Ramakrishna, *Energy Environ. Sci.* **2019**, *12*, 2148.
- [150] S. Zhai, H. E. Karahan, L. Wei, Q. Qian, A. T. Harris, A. I. Minett, S. Ramakrishna, A. K. Ng, Y. Chen, *Energy Storage Mater.* **2016**, *3*, 123.